# Characterizing the sediment provenance of East Antarctica's weak underbelly: The Aurora and Wilkes sub-glacial basins

Elizabeth L. Pierce,[1] Trevor Williams,[2] Tina van de Flierdt,[3] Sidney R. Hemming,[1,2] Steven L. Goldstein,[1,2] and Stefanie A. Brachfeld[4]

Received 31 January 2011; revised 5 August 2011; accepted 19 September 2011; published 10 December 2011.

[1] The Wilkes and Aurora basins are large, low-lying sub-glacial basins that may cause areas of weakness in the overlying East Antarctic ice sheet. Previous work based on ice-rafted debris (IRD) provenance analyses found evidence for massive iceberg discharges from these areas during the late Miocene and Pliocene. Here we characterize the sediments shed from the inferred areas of weakness along this margin (94°E to 165°E) by measuring $^{40}Ar/^{39}Ar$ ages of 292 individual detrital hornblende grains from eight marine sediment core locations off East Antarctica and Nd isotopic compositions of the bulk fine fraction from the same sediments. We further expand the toolbox for Antarctic IRD provenance analyses by exploring the application of $^{40}Ar/^{39}Ar$ ages of detrital biotites; biotite as an IRD tracer eliminates lithological biases imposed by only analyzing hornblendes and allows for characterization of samples with low IRD concentrations. Our data quadruples the number of detrital $^{40}Ar/^{39}Ar$ ages from this margin of East Antarctica and leads to the following conclusions: (1) Four main sectors between the Ross Sea and Prydz Bay, separated by ice drainage divides, are distinguishable based upon the combination of $^{40}Ar/^{39}Ar$ ages of detrital hornblende and biotite grains and the $\varepsilon_{Nd}$ of the bulk fine fraction; (2) $^{40}Ar/^{39}Ar$ biotite ages can be used as a robust provenance tracer for this part of East Antarctica; and (3) sediments shed from the coastal areas of the Aurora and Wilkes sub-glacial basins can be clearly distinguished from one another based upon their isotopic fingerprints.

**Citation:** Pierce, E. L., T. Williams, T. van de Flierdt, S. R. Hemming, S. L. Goldstein, and S. A. Brachfeld (2011), Characterizing the sediment provenance of East Antarctica's weak underbelly: The Aurora and Wilkes sub-glacial basins, Paleoceanography, *26*, PA4217, doi:10.1029/2011PA002127.

## 1. Introduction

### 1.1. East Antarctic Ice Sheet History

[2] Much of what we know about the evolution of the East Antarctic ice sheet (EAIS) comes from an examination of marine sediments. Much of what we know from marine sediments, however, tells us about changes in the ice sheet as a whole, rather than changes in a specific region, e.g., $\delta^{18}O$ recorded in benthic and planktic foraminera [*Shackleton and Kennett*, 1975; *Kennett and Shackleton*, 1976; *Kennett*, 1977; *Zachos et al.*, 1992, 1993, 2001; *Miller et al.*, 2005], $\delta^{18}O$ paired with Mg/Ca measurements in foraminifera [*Flower and Kennett*, 1994; *Lear et al.*, 2000; *Billups and Schrag*, 2002; *Billups and Schrag*, 2003; *Shevenell et al.*, 2004], the presence of ice-rafted debris (IRD) [*Kennett*, 1977], calibrating $\delta^{18}O$ records with sea level records [*Pekar and DeConto*, 2006], and seismic stratigraphy [*Escutia et al.*, 2005]. Due to the fact that 98% of East Antarctica is covered by thick ice, few areas exist where glacial features pre-dating the last glacial maximum are preserved at the surface (e.g., the Lambert Graben [*Hambrey and McKelvey*, 2000] and the Dry Valleys [*Marchant et al.*, 1993; *Lewis et al.*, 2006; *Lewis et al.*, 2007]), and hence many insights into past ice sheet dynamics in a given area have to rely on modeling studies [e.g., *Huybrechts*, 1993; *DeConto and Pollard*, 2003; *Hill et al.*, 2007].

[3] One way in which to evaluate the past stability of specific areas of the EAIS is to examine the provenance of glacially derived marine sediments. As ice flows over the continent, it erodes and entrains bedrock material. When the ice flow reaches the terminal point at the edge of the ice sheet, it can calve off into the ocean, forming icebergs that melt and drop their entrained material (IRD) as they travel in the ocean currents, [e.g., *Ruddiman*, 1977]. If the IRD possesses characteristics that allow it to be traced back to a specific geologic area, for example, based on geochemistry or lithology, the delivery and accumulation of IRD to the ocean floor can provide a means for identifying changes in ice sheet behavior that can be linked to a specific source

[1]Department of Earth and Environmental Sciences, Columbia University, New York, New York, USA.
[2]Lamont-Doherty Earth Observatory, Palisades, New York, USA.
[3]Department of Earth Science and Engineering, Imperial College London, London, UK.
[4]Department of Earth and Environmental Studies, Montclair State University, Montclair, New Jersey, USA.


0883-8305/11/2011PA002127

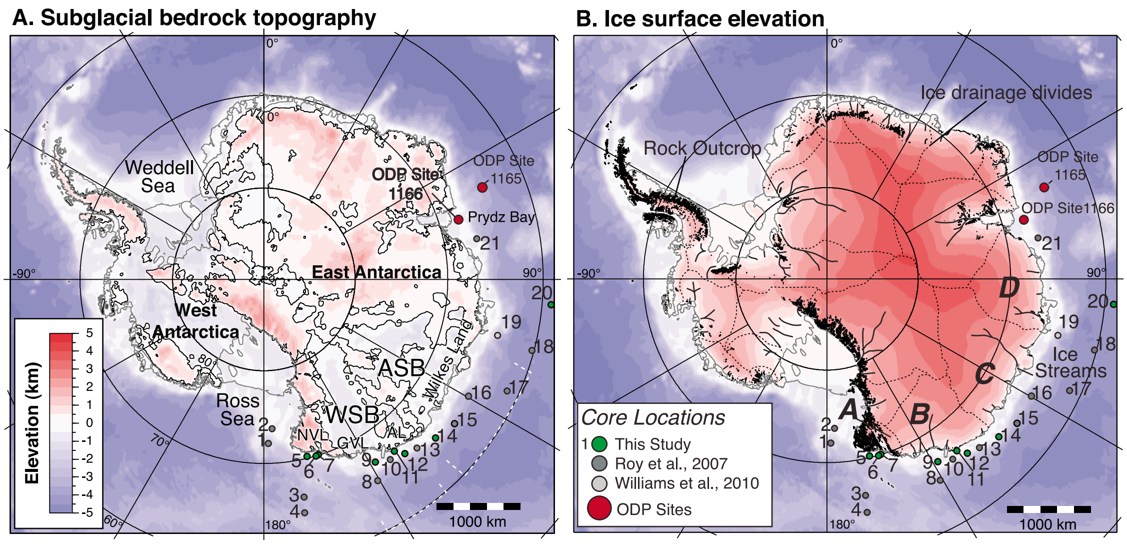


**Figure 1.** (a) Map showing marine sediment core locations and sub-glacial bedrock elevation [*Lythe et al.*, 2001] with the location of East Antarctic sub-glacial basins and seabed bathymetry (ETOPO-5). (b) Map of ice surface elevation (ETOPO-5), rock outcrop (Antarctic Digital Database), ice drainage divides [*Vaughan et al.*, 1999], and the approximate extent of major ice streams [*Bamber et al.*, 2000] (base map from *Williams et al.* [2010]). NVL, Northern Victoria Land; GVL, George V Land; AL, Adélie Land; QML, Queen Mary Land.

area, rather than the overall ice sheet. Geochemical provenance studies of IRD have been used successfully in the Northern Hemisphere to determine the source of the icebergs that delivered debris to the ocean, and thus the part of the ice sheet that underwent collapse [*Grousset et al.*, 1993; *Gwiazda et al.*, 1996; *Hemming et al.*, 1998, 2002; *Farmer et al.*, 2003; *Hemming*, 2004]. In general, studies that use geochemical characteristics of ice-rafted debris allow for a more detailed identification of source areas than studies of lithologic composition of the grains. The changing provenance of the IRD in the marine sediment record can then be interpreted in terms of past ice sheet dynamics [*Gwiazda et al.*, 1996; *Hemming et al.*, 2002; *Hemming*, 2004; *Williams et al.*, 2010].

[4] In this paper we focus on characterizing sediments shed from the margin of East Antarctica that lies between Prydz Bay and the Ross Sea (94°E to 165°E). There are two reasons that motivate us to study this particular area of East Antarctica. First, the low-lying Wilkes and Aurora sub-glacial basins are contained within this sector and drain along this part of the East Antarctic margin. These are potential areas of instability to the EAIS due to the fact that the majority of both basins lies more than 500 m below sea level [*Mercer*, 1978] (Figure 1). Second, previous evidence from a down-core study of the $^{40}Ar/^{39}Ar$ ages of individual ice-rafted hornblende grains in IRD-rich layers from Site 1165 of ODP Leg 188, located 400 km offshore of Prydz Bay and >1500 km west of this sector, has been interpreted to indicate past instability of the EAIS along the Wilkes and Adélie Land coasts [*Williams et al.*, 2010] (Figure 1). We find it significant that the inferred source areas of this IRD coincide with the two sectors of the EAIS that are underlain by the vast sub-glacial Wilkes and Aurora basins (Figure 1). If it is confirmed that these two sub-glacial basins have been a locus of weakness in the ice sheet during warmer times in the past, they may pose a threat to EAIS stability in the future as Earth continues to warm.

[5] Fundamental to any sedimentary provenance study is knowledge of the composition of potential source areas for the sediment that is being traced; this is a particular challenge in Antarctica where nearly the entire continent is covered by thick ice. By looking at glacially derived marine sediments near East Antarctica we aim to provide information pertaining to the geology that is covered, in addition to adding information to areas where limited outcrops have been previously studied. Large parts of the coastlines of the Wilkes and Aurora sub-glacial basins have no outcrops, and therefore marine sediments provide our sole window into their sub-glacial geology.

### 1.2. Geochemical Provenance Tools

#### 1.2.1. Nd Bulk Isotopes and $^{40}Ar/^{39}Ar$ Ages of Individual Minerals

[6] When choosing provenance tracers for a given sedimentary process, there are several important questions to consider. What are the potential lithologic sources of that tracer? Will all of the source areas be represented by this measurement, or will the measurement be biased toward a particular suite of rock types? To what extent are the source areas geochemically distinguishable from one another? In the case of mineral tracers, as in this study, it is important to consider what lithologies contain the minerals of interest, and if the minerals are a major constituent of those lithologies. Both hornblendes and biotites are major rock-forming minerals, and, combined, cover a wide spectrum of lithologies from felsic to mafic igneous rocks, and from low to high-grade metamorphic rocks. Neodymium (Nd) isotopes in the bulk fine fraction record the integrated signal of the source area, as Nd can be derived from essentially any lithology, though in varying concentrations depending upon

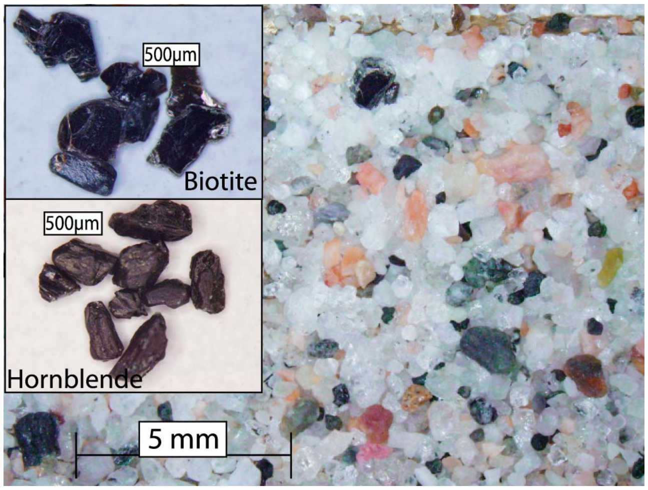


**Figure 2.** Photomicrograph of ice-rafted debris from the >150 $\mu$m size fraction in core ELT37–16. Inset: biotite and hornblende grains picked from the >150 $\mu$m size fraction. WSB, Wilkes Sub-glacial Basin; ASB, Aurora Sub-glacial Basin.

the source lithology [*Taylor and McLennan*, 1995; *Rudnick and Gao*, 2003].

[7] Since 98% of Antarctica is obscured by ice, our approach to characterizing source areas for sediments cannot be as direct as an approach used to characterize an exposed coastline, where the exact sample locations are known. Using $^{40}Ar/^{39}Ar$ hornblende ages, $^{40}Ar/^{39}Ar$ biotite ages, and bulk <63 $\mu$m $\varepsilon_{Nd}$ values in marine sediments, we can however place constraints on processes such as glacial-marine sedimentation and ice-rafting, and thus gain improved insights on geochemical provenance signatures. It is these signatures that we are trying to understand over the course of the evolution of the EAIS. Ice-rafting and the delivery of material by this process to a particular core site are ultimately dependent on the prevailing ocean currents. Around East Antarctica the westward flowing coastal current is the main transport mechanism for icebergs, potentially leading to a broad dispersal of IRD from a given sector. While *Roy et al.* [2007] found that icebergs around Antarctica today deposit IRD relatively close to their source area, material from one provenance sector could potentially be deposited offshore of another provenance sector.

[8] The advantage to combining individual mineral measurements with bulk isotope measurements is that measuring the $^{40}Ar/^{39}Ar$ ages of individual minerals allows for characterization of all end-members, while the bulk isotope measurements represent the integration of all end-members. Additionally, by using glacially derived sediments to characterize potential source areas, we are studying sediments that represent an integrated characterization of the lithology of a source area, even under ice cover. This way we can avoid any bias in characterizing source areas that would arise if we only looked at on-land point-source measurements, which may not represent the true range of lithologies or isotopic compositions.

[9] Limited outcrops and a circum-Antarctic core top survey measuring $^{40}Ar/^{39}Ar$ ages in hornblende grains [*Roy et al.*, 2007] allow for a systematic division of East Antarctica into several sectors based on the ages of known, major tectonothermal events. *Roy et al.* [2007] also measured the epsilon ($\varepsilon_{Nd}$) neodymium values of the < 63 $\mu$m fraction; $\varepsilon_{Nd}$ values are calculated as the deviation of the sample from the Chondritic Uniform Reservoir (CHUR) value ($^{143}Nd/^{144}Nd$ = 0.512638) [after *Jacobsen and Wasserburg*, 1980]

$$\varepsilon_{Nd} = \left[\frac{^{143}Nd/^{144}Nd_{sample}}{^{143}Nd/^{144}Nd_{CHUR}} - 1\right] \times 10,000.$$

*Roy et al.* [2007] identified the margin of East Antarctica from the Ross Sea west to Prydz Bay as a single “Wilkes Land” sector, owing to limited numbers of IRD grains in the western half of this sector. However, this sector can be divided into two separate provinces based on zircon U-Pb ages from Antarctic outcrops and from the counterpart provinces exposed in Australia [e.g., *Fitzsimons*, 2000].

[10] Previous work using $^{40}Ar/^{39}Ar$ hornblende ages as an IRD provenance tool inferred that the Wilkes and Adélie Land margins in East Antarctica were sources of IRD. Based on $^{40}Ar/^{39}Ar$ hornblende evidence for ca. 1100–1300 Ma sources in two layers and ca. 1500 Ma sources in a third layer from ODP Site 1165, *Williams et al.* [2010] reasoned that these two ages represent the Wilkes Land margin and the Adélie Coast, respectively, and potentially the Aurora and Wilkes sub-glacial basins. However, this inference was based on sparse source characterization data.

### 1.2.2. Biotite $^{40}Ar/^{39}Ar$ as an IRD Tracer

[11] In addition to providing an extensive new data set on $^{40}Ar/^{39}Ar$ ages of ice-rafted hornblende grains and bulk Nd isotopes, we investigated the potential for $^{40}Ar/^{39}Ar$ ages of individual biotite grains to be used as a tracer of IRD provenance in the Southern Ocean. First, initial observations of the > 150 $\mu$m size fraction of the piston core samples used in this study revealed that in addition to a large number of hornblende grains, there are also a large number of biotite grains in most samples (Figure 2). As both minerals are major rock-forming minerals, this is not particularly surprising. Second, $^{40}Ar/^{39}Ar$ ages can be reliably measured on biotites in the 63–150 $\mu$m size fraction because of their high potassium (and thus radiogenic argon) concentrations. This would make it possible to extend our studies to sites in the Southern Ocean where 63–150 $\mu$m biotite IRD grains are present in sufficient concentrations to define populations from the provenance source areas, but less-common >150 $\mu$m hornblende and biotite grains are not. Third, the combination of hornblende and biotite $^{40}Ar/^{39}Ar$ ages from the glacially derived sediment in the piston cores is valuable because hornblende begins to retain $^{40}Ar$ at ~500°C, while biotites begin to retain $^{40}Ar$ at ~300°C [*Reiners et al.*, 2005]. Given the polymetamorphic history of East Antarctica, using two thermochronometers to further constrain the geologic age provenances could be advantageous as we may be able to apply these data to infer the metamorphic history of East Antarctica. Furthermore, the biotites may have ages different from the hornblendes, due either to the cooling rate following the last tectonothermal event, low temperature re-setting of the $^{40}Ar/^{39}Ar$ biotite ages, or both, which could potentially allow for further refinement of the provenance sectors that we are trying to characterize. Finally, by analyzing both biotites and hornblendes, we are increasing our representation of source

areas as these two minerals collectively represent a wide array of lithologies. Hence we can also assess any lithological bias in the provenance data from one mineral alone.

### 1.3. Goals for This Study

[12] Our goals for this study are: (1) to provide detailed constraints on the geochemical characterizations ($^{40}Ar/^{39}Ar$ and Nd isotopic composition) of the terrigenous material shed from the ice sheet in the inferred areas of past East Antarctic ice sheet instability between 94° and 165°E, which includes the Wilkes and Aurora sub-glacial basins. In order to provide a robust geochemical framework for the interpretation of EAIS evolution, we refine the *Roy et al.* [2007] study, which characterized this margin of East Antarctica as one provenance sector based upon sparse individual $^{40}Ar/^{39}Ar$ hornblende and $\varepsilon_{Nd}$ measurements, and (2) to explore the use of $^{40}Ar/^{39}Ar$ biotite ages for IRD provenance studies in East Antarctica. In addition to evaluating $^{40}Ar/^{39}Ar$ biotite ages for characterizing the source areas between 94° and 165°E, we also present $^{40}Ar/^{39}Ar$ ages of ice-rafted biotite grains from the same depositional layers that *Williams et al.* [2010] used for measuring $^{40}Ar/^{39}Ar$ hornblende ages.

## 2. Importance of the Wilkes and Aurora Sub-glacial Basins

[13] The Wilkes and Aurora basins of East Antarctica are large, low-lying sub-glacial basins extending from the center of the East Antarctic continent toward the George V/Adélie and Wilkes Land coastlines, respectively. The inference that these basins are potential foci for past and future ice sheet instability is based upon their elevation below sea level [*Mercer*, 1978; *Drewry*, 1983] (Figure 1), the presence of many sub-glacial lakes in the hinterland [*Siegert et al.*, 2005a], and the hydrologic connection between the sub-glacial lakes and the margins of the ice sheet [*Siegert et al.*, 2005a, 2005b; *Wingham et al.*, 2006; *Jordan et al.*, 2010]. It is becoming increasingly apparent that sub-glacial water plays an important role in ice dynamics [*Bell*, 2008], and further studies of the link between the sub-glacial lakes, the Wilkes and Aurora sub-glacial basins and ice sheet dynamics are an important goal for future studies of EAIS stability. Potential links between these are developed by *Erlingsson* [1994] and *Alley et al.* [2006], who both presented models for ice sheets overriding and "capturing" lakes, which subsequently leads to the growth of the sub-glacial lake due to melting, in turn leading to jökuhlaups, and finally to ice stream surges. Evidence for instability in these regions also comes from modeled studies of past ice sheet behavior [e.g., *Huybrechts*, 1993; *Hill et al.*, 2007], which show that warming leads to initial retreat of the EAIS in these regions. Even models that predict a relatively stable EAIS have some ice margin retreat in these areas [*Pollard and DeConto*, 2009].

[14] Evidence from the marine sedimentary record for instabilities in this region comes from *Williams et al.* [2010], who argue for the collapse of ice streams feeding from these areas, leading to massive discharges of icebergs during the late Miocene and Early Pliocene, as the best explanation for far-traveled ice-rafted hornblende grains observed at ODP Site 1165 in Prydz Bay (Figure 1). The $^{40}Ar/^{39}Ar$ hornblende ages from eight IRD layers in ODP Site 1165, spanning the Early Miocene to mid-Pliocene (19–3.5 Ma), show significant changes in provenance that are interpreted to reflect dynamic instability of the EAIS during warmer intervals [*Williams et al.*, 2010].

## 3. Sample Locations and Methods

### 3.1. Marine Sediment Core Locations and Sample Selection

[15] The 16 core locations investigated are primarily located on the continental shelf, and form a transect around the perimeter of East Antarctica from 94° to 165°E, encompassing from west to east the Queen Mary Land, Wilkes Land, Adélie Coast, George V Land and Northern Victoria Land sectors.

[16] Nine of the 16 samples provided by the Antarctic Marine Geology Repository at Florida State University (see Table S1) yielded sufficient terrigenous sediment from the bottom layer of the piston core for analyses.[1] We targeted the bottom layers of piston cores with the idea that these layers might be more likely to be rich in terrigenous material, assuming such layers would be difficult to penetrate with a piston core. We also assumed that the piston cores would not be able to penetrate far into glacial diamict, and that thus the samples would be no older than Last Glacial Maximum (LGM) in age. Further preliminary biostratigraphic study of the samples (C. Sjunneskog, Antarctic Marine Geology Research Facility, personal communication, 2011) has revealed the ages for samples from Cores 5 and 15 (DF80–35 and ELT37–16) to be LGM/Holocene. The ages for the samples from Cores 7 (DF80–34) and 20 (ELT49–30) are however ~2.8–2.1 Ma and ~2–4 Ma, respectively (see Figure 1 and Table 1 for site locations). Further work is underway to constrain the ages of these samples. The working hypothesis that the bottom layers of piston cores would yield more terrigenous material was supported by the fact that we were able to find significantly more hornblendes from the core-bottom samples than *Roy et al.* [2007] found in core top samples (see Cores 12 and 14 in Table 1). In addition to the core bottom samples, we sampled 2 layers (2305 and 2370 cm) of LGM glacial diamict from sample location NBP01-01-JPC11 (Core 11, offshore Adélie Land; Figure 1 and Table 1) [*Leventer et al.*, 2006].

[17] In order to determine the viability of $^{40}Ar/^{39}Ar$ biotite ages as a provenance tool for IRD in the Southern Ocean (see section 1.2.2) we measured biotites (63–150 $\mu$m and >150 $\mu$m) from the same piston core samples discussed above for comparison with the $^{40}Ar/^{39}Ar$ hornblende ages. While we would not expect there to be a difference in the $^{40}Ar/^{39}Ar$ biotite ages from these two size fractions, we have measured $^{40}Ar/^{39}Ar$ biotite ages from both because (1) we traditionally have measured grains only in the >150 $\mu$m fraction and (2) to eliminate any uncertainty that there might be a difference. As a second evaluation of the potential of biotite $^{40}Ar/^{39}Ar$ ages as an IRD tracer we analyzed biotites (>150 $\mu$m) from the same layers in ODP Site 1165 that were analyzed for hornblende $^{40}Ar/^{39}Ar$ ages by *Williams et al.* [2010], with depositional ages of 3.5, 4.65, 7.0 and 19.0 Ma (note that the 4.65 Ma depositional layer was originally reported by *Williams et al.* [2010] to have an age of 4.8 Ma;

[1]Auxiliary materials are available at ftp://ftp.agu.org/apend/pa/2011PA002127.

**Table 1.** Summary of $^{40}Ar/^{39}Ar$ Ages and Neodymium Isotope Measurements Around the East Antarctic Perimeter

| Sample Code | Sample | Latitude | Longitude | Sector[a]/ Drainage[b]/ Basin[c] | Study[d] | Mineral[e] | Number of Grains in the Following Age Group (in Ma)[f] 0–50 | 300–400 | 400–550 | 1000–1300 | 1400–1500 | 1500–1800 | 2000–2500 | Other | Total | $\varepsilon_{Nd}$[g] |
|---|---|---|---|---|---|---|---|---|---|---|---|---|---|---|---|---|
| 1 | ELT27–20 | −71.96 | 178.60 | NVL/***A***/n | R[4] | Hb | 1 | 1 | 7 | - | - | - | - | 5 | 14 | −6.9 |
| 2 | NBP9802–2H | −73.54 | 176.96 | NVL/***A***/n | R | Hb | - | - | 4 | 1 | - | - | - | - | 5 | −7.3 |
| 3 | NBP9802–4H | −64.20 | 170.08 | NVL/***A***/n | R | Hb | - | 1 | - | - | - | - | - | 3 | 4 | −2.7 |
| 4 | NBP9802–3H | −66.14 | 169.45 | NVL/***A***/n | R | Hb | - | - | 1 | - | - | - | - | 2 | 3 | ~ |
| 5 | DF80–35 (269–273) | −70.02 | 166.42 | NVL/***A***/n | P | Hb | 14 | 2 | 3 | - | - | - | - | 2 | 21 | ~ |
| | | | | | | B (>150) | - | 10 | 2 | - | - | - | - | - | 12 | |
| | | | | | | B (63–150) | - | 9 | 1 | - | - | - | - | 1 | 11 | |
| 6 | DF80–20 (160–164) | −69.78 | 163.68 | NVL/***A***/n | P | Hb | 1 | 3 | 2 | - | - | - | - | 2 | 8 | −10.3 |
| | | | | | | B (>150) | - | 14 | 4 | 3 | - | - | - | 3 | 24 | |
| | | | | | | B (63–150) | - | 8 | 3 | - | - | - | - | 3 | 14 | |
| 7 | DF80–34 (222–226) | −69.92 | 162.83 | NVL/***A***/n | P | Hb | 9 | - | 16 | 3 | - | - | - | 8 | 36 | −3.5 |
| | | | | | | B (>150) | - | 4 | 12 | 1 | - | - | - | 6 | 23 | |
| | | | | | | B (63–150) | - | 3 | 6 | - | - | - | - | 1 | 10 | |
| 8 | ELT37–04 | −64.83 | 150.49 | GVL, AL/***B***/WSB | R[4] | Hb | ~ | ~ | ~ | ~ | ~ | ~ | ~ | ~ | ~ | −12.4 |
| 9 | DF79–47 (563–567) | −66.67 | 148.73 | GVL, AL/***B***/WSB | P | Hb | 1 | - | 15 | 4 | 7 | 8 | - | 11 | 46 | −12.4 |
| | | | | | | B (63–150) | - | - | 8 | - | - | - | - | 2 | 10 | |
| 10 | ELT37–06 | −66.08 | 145.02 | GVL, AL/***B***/WSB | R | Hb | 2 | - | 2 | - | - | 3 | - | 1 | 8 | −17.0 |
| 11 | NBP0101 JPC11 2305–2310 | −66.56 | 143.05 | GVL, AL/***B***/WSB | P[5] | Hb | - | - | - | 1 | 2 | 11 | 1 | - | 15 | −23.6 |
| | | | | | | B (>150) | - | - | - | - | - | 14 | - | - | 14 | |
| 11 | NBP0101 JPC11 2370–2375 | −66.56 | 143.05 | GVL, AL/***B***/WSB | P | Hb | - | - | - | 1 | 3 | 22 | 6 | 9 | 41 | ~ |
| | | | | | | B (>150) | - | - | - | - | - | 15 | - | - | 15 | |
| 12 | ELT37–09 (140–144) | −65.55 | 141.10 | GVL, AL/***B***/WSB | P | Hb | 1 | 1 | 2 | - | 3 | 27 | - | 11 | 45 | −21.1 |
| | | | | | | B (>150) | - | 2 | 33 | 1 | - | 8 | - | 5 | 48 | |
| | | | | | | B (63–150) | - | - | 3 | 1 | - | 6 | - | - | 10 | |
| 12 | ELT37–09 A (137–139) | −65.55 | 141.10 | GVL, AL/***B***/WSB | P | B (>150) | - | - | 6 | - | 2 | 5 | - | 1 | 14 | ~ |
| 12 | ELT37–09 B (92–93) | −65.55 | 141.10 | GVL, AL/***B***/WSB | P | B (>150) | - | - | 7 | - | - | 7 | - | - | 14 | ~ |
| 12 | ELT37–09 | −65.55 | 141.10 | GVL, AL/***B***/WSB | R[4] | Hb | 2 | - | 4 | 1 | 4 | 24 | 1 | 6 | 42 | −20.4 |
| 13 | ELT37–10 | −65.22 | 137.88 | GVL, AL/***B***/WSB | R | Hb | ~ | ~ | ~ | ~ | ~ | ~ | ~ | ~ | ~ | −16.1 |
| 14 | ELT37–13 | −64.67 | 132.98 | WL/***C***/ASB | R | Hb | 1 | - | - | 7 | 3 | 2 | - | 2 | 15 | −14.9 |
| 14 | ELT37–13 (113–120) | −64.67 | 132.98 | WL/***C***/ASB | P | Hb | - | - | 1 | 39 | 1 | 1 | 2 | 3 | 47 | −14.7 |
| | | | | | | B (>150) | - | - | - | 15 | 1 | 1 | - | - | 17 | |
| | | | | | | B (63–150) | - | - | - | 11 | - | - | - | 1 | 12 | |
| 15 | ELT37–16 (231–235) | −63.97 | 127.4 | WL/***C***/ASB | P | Hb | - | 1 | - | 32 | 9 | 11 | 4 | 6 | 63 | −13.4 |
| | | | | | | B (>150) | - | - | - | 41 | 1 | - | 1 | 3 | 46 | |
| | | | | | | B (63–150) | - | 1 | - | 8 | 1 | - | - | - | 10 | |
| 16 | ELT50–18 | −64.43 | 119.98 | WL/***C***/ASB | R | Hb | ~ | ~ | ~ | ~ | ~ | ~ | ~ | ~ | ~ | −12.3 |
| 17 | ELT50–16 | −61.04 | 114.81 | WL/***C***/ASB | R | Hb | - | - | 1 | 6 | - | 1 | - | 1 | 9 | −13.9 |
| 18 | ELT50–13 | −60.00 | 105.00 | WL/***C***/ASB | R[4] | Hb | - | - | - | 1 | - | - | - | 1 | 2 | −14.8 |

**Table 1.** (continued)

| Sample Code | Sample | Latitude | Longitude | Sector[a]/ Drainage[b]/ Basin[c] | Study[d] | Mineral[e] | Number of Grains in the Following Age Group (in Ma)[f] 0–50 | 300–400 | 400–550 | 1000–1300 | 1400–1500 | 1500–1800 | 2000–2500 | Other | Total | $\varepsilon_{Nd}$[g] |
|---|---|---|---|---|---|---|---|---|---|---|---|---|---|---|---|---|
| 19 | DSDP 268 | −63.9 | 105.2 | WL/***C***/ASB | W | Hb | - | - | 1 | 23 | - | - | - | 8 | 32 | ~ |
| 20 | ELT49–30 (1698–1702) | −59.01 | 95.23 | QML/***D***/n | P | Hb | 2 | - | - | 26 | 1 | - | - | 5 | 33 | −12.3 |
| | | | | | | B (>150) | 1 | - | 9 | 6 | - | - | - | 4 | 20 | |
| | | | | | | B (63–150) | - | - | 3 | 4 | - | - | - | 3 | 10 | |
| 21 | ELT47–07 | −66.66 | 77.90 | QML/***D***/n | R[4] | Hb | - | - | 32 | 3 | - | 1 | - | 18 | 54 | −21.3 |

[a]Sectors refer to the geographic sectors that the core sample is located offshore from. NVL, Northern Victoria Land; GVL, George V Land; AL, Adélie Land; WL, Wilkes Land; QML, Queen Mary Land. Samples are core tops unless depth () values are given, in which case the samples are from the bottom layer of a piston core.

[b]Drainage divides (*A*, ~158°E to ~180°E; *B*, ~133°E to ~158°E; *C*, ~103°E to ~133°E; *D*, ~73°E to ~103°E) are based on the ice drainages from *Vaughan et al.* [1999] (see Figure 1).

[c]Indicates which subglacial basin sediment in this core represents; WSB, Wilkes Subglacial Basin (~135°E to 155°E); ASB, Aurora Subglacial Basin (~133°E to ~105°E); n, neither basin.

[d]Values are from the following studies (P, this study; R[4], $\varepsilon_{Nd}$ [from *van de Flierdt et al.*, 2008]; R, *Roy et al.* [2007]; B, *Brachfeld et al.* [2007]; W, *Williams et al.* [2010].

[e]Mineral on which $^{40}Ar/^{39}Ar$ age was measured. Hb, hornblende; B (>150), biotite > 150 $\mu$m; B (63–150), biotite 63–150 $\mu$m.

[f]Age ranges were determined based upon the dominant populations observed in the $^{40}Ar/^{39}Ar$ data; the 0–50 Ma (young volcanics from the Ross Sea/Victoria Land); 300–400 Ma (Bowers Mountain terrane); 400–550 Ma (the Ross orogeny); 1400–1500 Ma (Mertz Shear zone age); 1000–1300 Ma (Grenville orogeny); 1500–1800 Ma and 2000–2500 Ma (thermal events in Adélie Land) ("-" are zero grains in this age category; "~" are no grains measured).

[g]$\varepsilon_{Nd}$ values were measured on the bulk < 63 $\mu$m fraction for studies labeled "P," and on the terrigenous < 63 $\mu$m fraction for studies marked R and B. Calculations are based on the chondritic values of $^{143}Nd/^{144}Nd$ = 0.512638 [*Jacobsen and Wasserburg*, 1980] (see Data Set S2).

the age has since been refined to 4.65 Ma). The exact part of the core containing an interesting 1500 Ma population of $^{40}Ar/^{39}Ar$ hornblende ages during the IRD event at 4.65 Ma was completely sampled and hence we picked another layer, 1165B-6H1(70 cm), 30 cm upcore. This layer was also analyzed by *Williams et al.* [2010] as part of a sequence of samples spanning the "4.8 Ma event."

### 3.2. $^{40}Ar/^{39}Ar$ Dating and $^{143}Nd/^{144}Nd$ Analyses

[18] Bulk samples were dried, disaggregated and dispersed in de-ionized water, and sieved into the following size fractions: <63 $\mu$m, 63 to 150 $\mu$m and 150 $\mu$m to 1 mm. Following magnetic separations, hornblendes and biotites were handpicked (n > 30 when possible) from the 150 $\mu$m to 1 mm size fraction, with additional biotites picked from the 63–150 $\mu$m size fraction. Hornblendes, biotites and standards were irradiated either at the Cd-lined in-core facility (CLICIT) at the Oregon State rector, or (also with Cd shielding) at the U.S. Geological Survey (USGS) TRIGA reactor in Denver, CO. $^{40}Ar/^{39}Ar$ ages were obtained using single-step $CO_2$ laser fusion at the Lamont-Doherty Earth Observatory (L-DEO) argon geochronology lab (AGES: Argon Geochronology for the Earth Sciences). J values used to correct for neutron flux were calculated using the co-irradiated Mmhb-1 hornblende standard (525 Ma [*Samson and Alexander*, 1987]).

[19] Neodymium isotopes were measured on the bulk <63 $\mu$m size fraction. For this study we did not remove any authigenic phases prior to analysis, because the Nd budget of marine sediments located close to the continent is assumed to be dominated by the terrigenous component. This assumption was confirmed to be valid as our Nd isotopic compositions from two sites that were previously analyzed by *Roy et al.* [2007] (samples that were leached prior to analyses) agree within error.

[20] Approximately 0.1 g ± 0.5% of sample and 0.4 g ± 0.5% of lithium metaborate flux were weighed and mixed, and samples were fused at 1050°C for 30 min. The molten sample was then dropped into 50 mL of 7% $HNO_3$ in a Teflon beaker and placed on a stir plate for 15 min to ensure dissolution. The pH of the samples was adjusted to 8 (using ammonium hydroxide) to precipitate iron, and co-precipitate the rare earth elements (REE). This approach leaves soluble elements such as boron and lithium from the flux and sodium, potassium and calcium from the sample in solution and thus reduces the ion load on the cation exchange column. Precipitates were rinsed with de-ionized water, and re-dissolved in 2N HCl. Neodymium was subsequently separated from the matrix by a two-step ion chromatography. Seven mL columns filled with AG50W-8X cation resin were used to separate the REE from the matrix. The columns were cleaned with 10 mL of 4N $HNO_3$, equilibrated with 5 mL of 2N HCl, and the REEs were eluted with 10 mL of 4N $HNO_3$. The REE aliquot was dried down, taken up in 0.22N $HNO_3$, and then passed through 800 $\mu$L columns filled with Eichrom Ln-Spec resin to isolate the Nd from the other REEs. The columns were first cleaned with 6 mL of 3 N HCl, conditioned twice with 1 mL 0.22N $HNO_3$, and the Nd was eluted with 5.5 mL of 0.22N $HNO_3$. Neodymium isotope measurements were carried out in a static mode on the VG Axiom MC-ICP-MS at L-DEO. A $^{146}Nd/^{144}Nd$ ratio of 0.7219 was applied to correct for instrumental mass

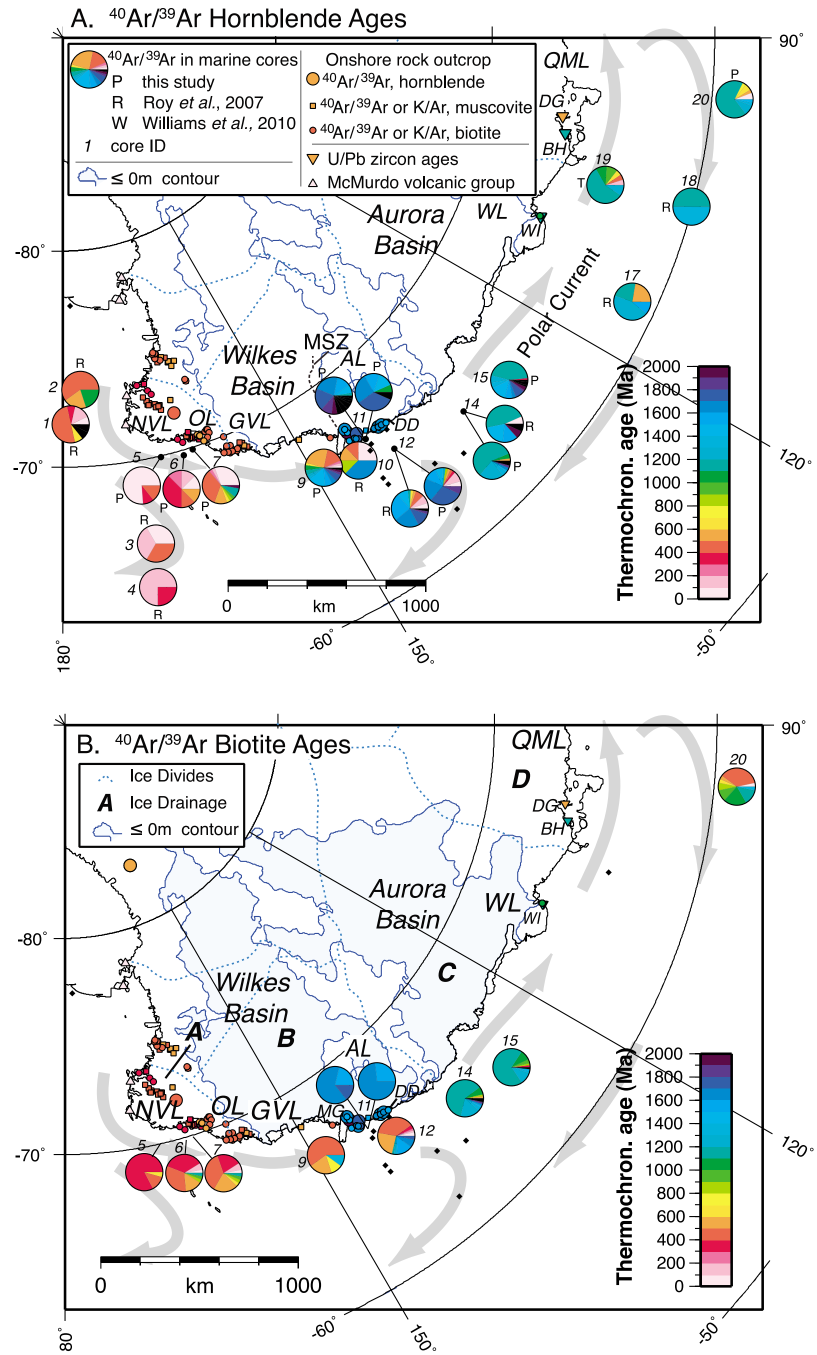


**Figure 3.** Map of thermochronologic data from marine sediment cores and on-land ages along the margin of East Antarctica (90°E to 180°) (a) $^{40}Ar/^{39}Ar$ hornblende ages from marine sediment cores and (b) $^{40}Ar/^{39}Ar$ biotite ages from marine sediment cores. Each pie chart represents the population of ages at that site with each equal-area wedge representing one analysis. The onshore $^{40}Ar/^{39}Ar$ hornblende thermochronology [*Di Vincenzo et al.*, 2007; *Duclaux et al.*, 2007; *Goodge*, 2007; *Phillips et al.*, 2007; *Wilson et al.*, 2007] is supplemented with $^{40}Ar/^{39}Ar$ biotite and muscovite data [*Adams*, 2006]. In areas lacking Ar data, zircon U–Pb data are plotted [*Black et al.*, 1992; *Sheraton et al.*, 1992; *Boger et al.*, 2000; *Carson et al.*, 2000; *Post*, 2000; *Möller et al.*, 2002; *Liu et al.*, 2006; *Liu et al.*, 2007]. Diamond symbols mark DSDP and IODP sites. Ice-drainage divides (A-D) [*Vaughan et al.*, 1999] and the 0 m sub-glacial contour line [*Lythe et al.*, 2001] outlining the Wilkes and Aurora basins are shown in light and dark blue, respectively. NVL, Northern Victoria Land; OL, Oates Land; GVL, George V Land; AL, Adélie Land; DD, Dumont D'urville; MG, Mertz Glacier; WL, Wilkes Land; QML, Queen Mary Land; WI, Windmill Islands; BH, Bunger Hills; DG, Denman Glacier; MSZ, Mertz Shear Zone (extent of MSZ from *Ferraccioli et al.* [2009]).

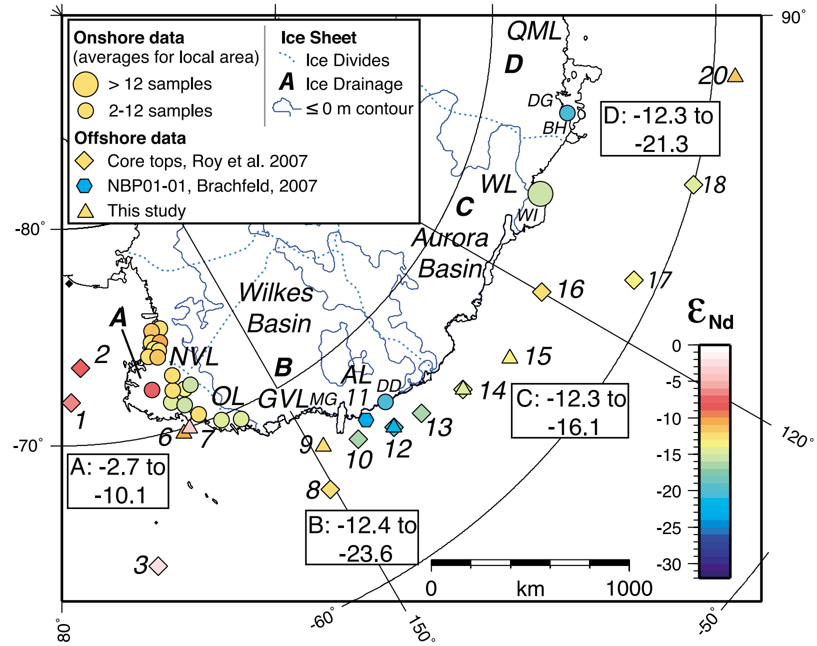


**Figure 4.** Epsilon neodymium ($\varepsilon_{Nd}$) values (T = 0 Ma) from marine cores and from on-land samples. Outcrop data from BH [*Sheraton et al.*, 1990], WI [*Möller et al.*, 2002], DD [*Peucat et al.*, 1999], NVL/OL [*Borg et al.*, 1987; *Rocchi et al.*, 1998; *Henjes-Kunst and Schüssler*, 2003]. NVL, Northern Victoria Land; OL, Oates Land; GVL, George V Land; AL, Adélie Land; DD, Dumont D'Urville; MG, Mertz Glacier; WL, Wilkes Land; QML, Queen Mary Land; WI, Windmill Islands; BH, Bunger Hills; DG, Denman Glacier. Ice-drainage divides [*Vaughan et al.*, 1999] and the 0 m sub-glacial contour line [*Lythe et al.*, 2001] outlining the Wilkes and Aurora basins are shown in light and dark blue, respectively.

bias following the exponential law. Tests with doped standards showed that interferences from $^{144}$Sm are adequately corrected, if the $^{144}$Sm contribution is less than 0.1% of the $^{144}$Nd signal. Samarium contributions of all our samples were significantly below that level. Repeated analyses of the JNdi standard during the two measurement sessions yielded $^{143}$Nd/$^{144}$Nd ratios of 0.512116 ± 0.000020 (2$\sigma$ S.D., n = 11) and 0.512097 ± 0.000013 (2$\sigma$ S.D., n = 13). Since standards showed a drift over both analytical sessions, we bracketed sample runs by two standards on each side. Correction factors for samples were determined from averaged value of each set of four standards relative to the accepted JNdi value of 0.512115 (equivalent to a La Jolla value of 0.511858 [*Tanaka et al.*, 2000]).

## 4. Results

### 4.1. Marine Sediment Core Survey Around the East Antarctic Perimeter

[21] We have measured an average of 78 (minimum of 29, maximum of 119) $^{40}$Ar/$^{39}$Ar ages on individual hornblende and biotite grains from 8 marine sediment cores, in addition to measuring the $\varepsilon_{Nd}$ of the bulk fine fraction from each sample. These measurements quadruple the number of detrital $^{40}$Ar/$^{39}$Ar analyses from glacial-marine sediments along this margin of East Antarctica.

[22] $^{40}$Ar/$^{39}$Ar hornblende and biotite ages and neodymium isotopic compositions from the marine sediment cores are summarized in Table 1, along with data on $^{40}$Ar/$^{39}$Ar hornblende ages and neodymium isotopic compositions of the fine fraction from *Roy et al.* [2007] and *van de Flierdt et al.* [2008]. $^{40}$Ar/$^{39}$Ar hornblende and biotite results are shown in Figure 3; neodymium isotope measurements are shown in Figure 4, and $^{40}$Ar/$^{39}$Ar hornblende and biotite ages by core location are shown in Figure 5. Full results for all measurements are summarized in Figure 6 and can be found in Appendices B and C.

[23] Three dominant $^{40}$Ar/$^{39}$Ar age populations appear in our data: 400–550 Ma (Northern Victoria Land, George V Land and Prydz Bay), 1100–1200 Ma (Wilkes Land) and 1500–1800 Ma (Adélie Land), with 3 grains ~2500 Ma present in cores proximal to Adélie Land. Additional age populations include a < 50 Ma hornblende population, in which the majority are < 15 Ma, and a 300–400 Ma biotite population in cores off the coast of Northern Victoria Land (Table 1 and Figure 3). Neodymium isotope measurements span a range of ~20 epsilon units from radiogenic values off Oates Land ($\varepsilon_{Nd}$ = −3.3) to very unradiogenic values off Adélie Land ($\varepsilon_{Nd}$ = −23.6) (Figure 4).

### 4.2. $^{40}$Ar/$^{39}$Ar Biotite Ages From ODP Site 1165 (>150 $\mu$m Size Fraction)

[24] Biotites were picked from the >150 $\mu$m size fraction of each of the four downcore samples, in order to compare the $^{40}$Ar/$^{39}$Ar age distribution of the biotites with those of the hornblendes previously analyzed. Each sample contains a population of 450–550 Ma $^{40}$Ar/$^{39}$Ar biotites ages, and an

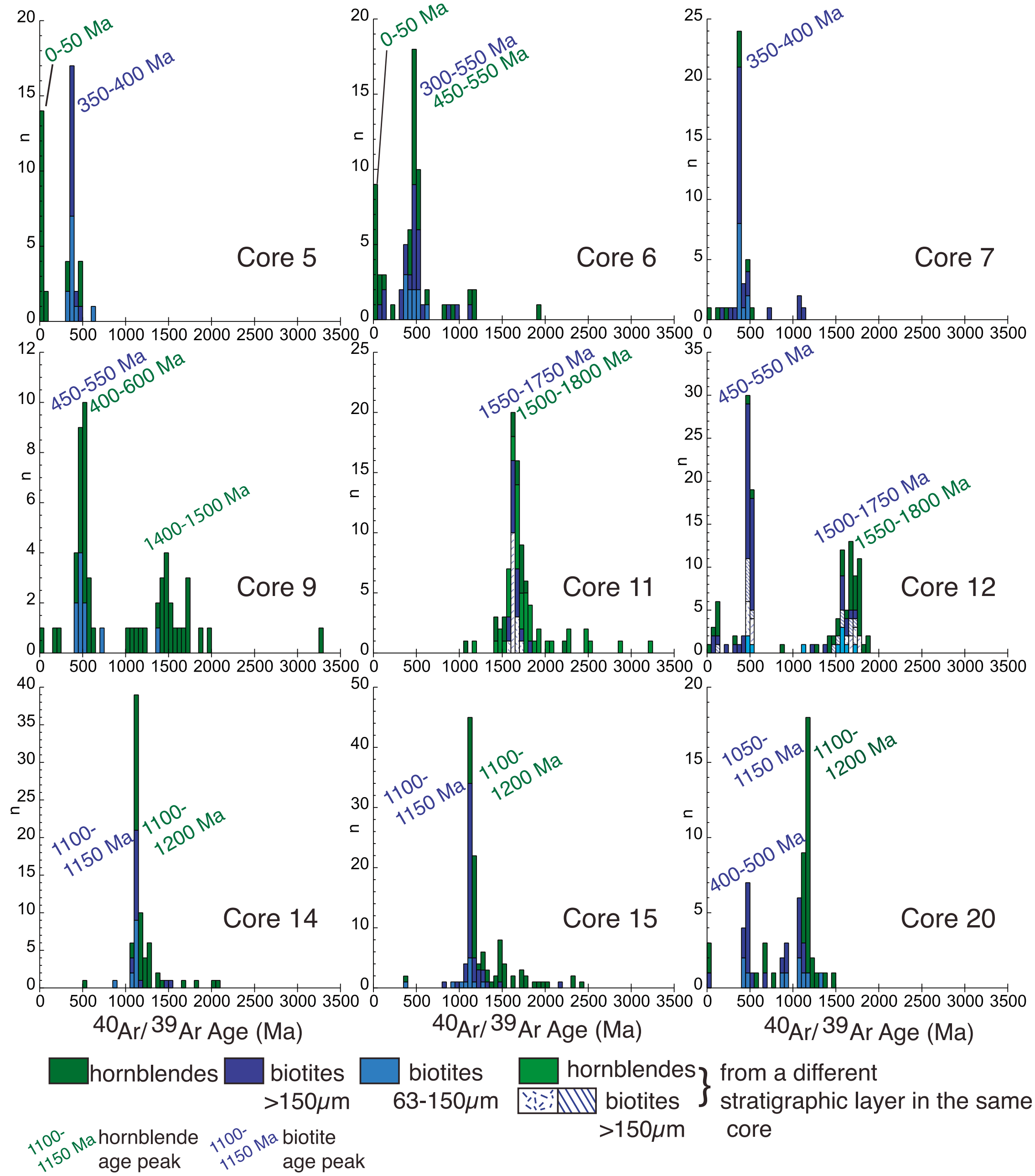


**Figure 5.** $^{40}Ar/^{39}Ar$ hornblende (green) and biotite (blue) ages from piston cores samples showing the general agreement in ages between hornblende (>150 $\mu$m) and biotites (63–150 $\mu$m and >150 $\mu$m) (see text).

additional population 1100–1200 Ma of $^{40}Ar/^{39}Ar$ biotite ages (Figure 7).

## 5. Discussion

### 5.1. Characterization of IRD Source Areas

#### 5.1.1. Geochemical Characterization of Ice Drainage Divides

[25] Our new measurements of detrital $^{40}Ar/^{39}Ar$ hornblende and biotite grains and $\varepsilon_{Nd}$ values allow us to identify 4 geologic provinces between 94°E and 165°E. As two of these geologic sectors coincide with ice sheet drainages, and given our interest in applying these data to past studies of EAIS dynamics, we discuss our data in the context of the 4 ice drainage divides, described by *Vaughan et al.* [1999], that terminate at the East Antarctic margin between the Ross Sea and Prydz Bay (see Table 1 and Figure 6).

[26] *Vaughan et al.* [1999] improved upon the ice-flow and drainage basin divides of *Giovinetto and Bentley* [1985] and *Drewry* [1983], providing more accurate though not drastically different boundaries for the 26 drainage basins in Antarctica. We have labeled the four basins that drain to our study area (the D′D″, DD′, C′D, CC′ basins of *Vaughan et al.* [1999]) as *A* (~158°E to ~172°E), *B* (~133°E to ~ 158°E), *C* (~103°E to ~ 133°E), and *D* (~73°E to ~103°E), respectively (Figure 6). These four drainage basins combined cover

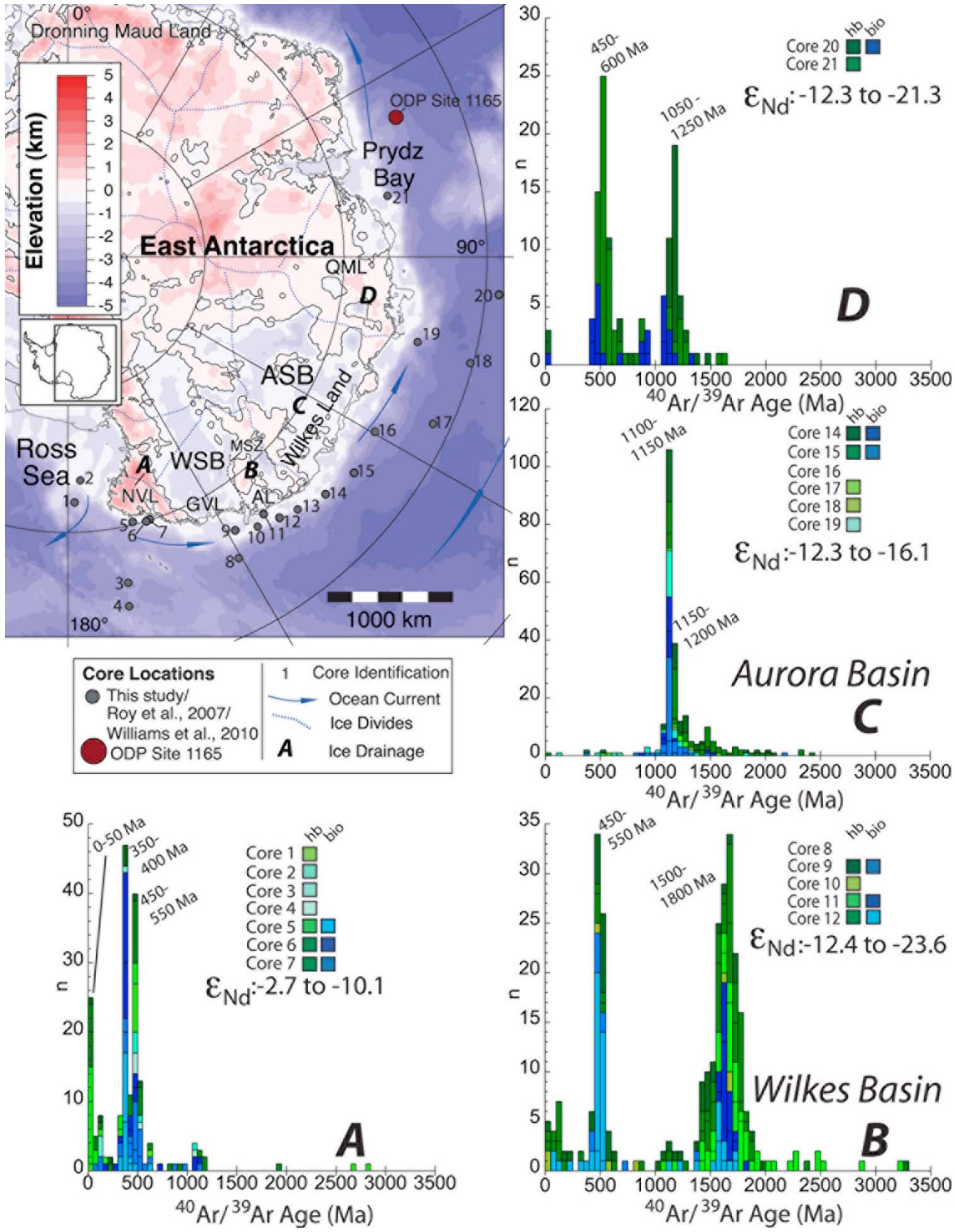


**Figure 6.** Geochemistry of ice-flow drainages and the Wilkes (WSB) and Aurora (ASB) basins based upon $^{40}Ar/^{39}Ar$ hornblende (>150 $\mu$m) ages, $^{40}Ar/^{39}Ar$ biotite (>150 $\mu$m and 63–150 $\mu$m) ages, and epsilon neodymium ($\varepsilon_{Nd}$) values. The letters A–D signify divisions of the ice sheet drainage system (ice sheet drainage from *Vaughan et al.* [1999]). Histograms (50 Ma bins) show $^{40}Ar/^{39}Ar$ hornblende and biotites ages from samples grouped by the ice-drainage that is proximal to the cores. Map of bedrock topography modified from *Williams et al.* [2010]. NVL, Northern Victoria Land; GVL, George V Land; AL, Adélie Land; MSZ, Mertz Shear Zone [*Ferraccioli et al.*, 2009]; Hb (green), hornblende ages; Bio (blue), biotite ages.

a total area of 2619 × $10^3$ km$^2$ ($A$ = 710 × $10^3$ km$^2$, $B$ = 684 × $10^3$ km$^2$, $C$ = 1169 × $10^3$ km$^2$, and $D$ = 156 × $10^3$ km$^2$) out of which ~ 1,110 × $10^3$ km$^2$ are below sea level.

[27] Previously published onshore data are summarized in Figures 3 ($^{40}Ar/^{39}Ar$ and U-Pb) and 4 (Nd). Based on the onshore thermochronology data, four age sectors can be identified: (1) The Western Ross Sea, Northern Victoria Land, and Oates Land, which are characterized by $^{40}Ar/^{39}Ar$ and U-Pb ages of ~400–600 Ma, with a smaller population of younger $^{40}Ar/^{39}Ar$ ages from the McMurdo Volcanic Group in the western Ross Sea; (2) The Mertz Shear Zone and Adélie Land, which are characterized by $^{40}Ar/^{39}Ar$ and U-Pb zircons ages of >1500 Ma; (3) Wilkes Land, which is characterized by U-Pb zircon ages of 1100–1300 Ma (based on outcrop data from two ice free areas only); and (4) Queen Mary Coast, which contains the boundary between rocks with 1100–1300 Ma ages and rocks showing Pan-African overprinting of ~500 Ma (Figure 3, references are listed in the caption; see *Williams et al.* [2010] for a summary with references).

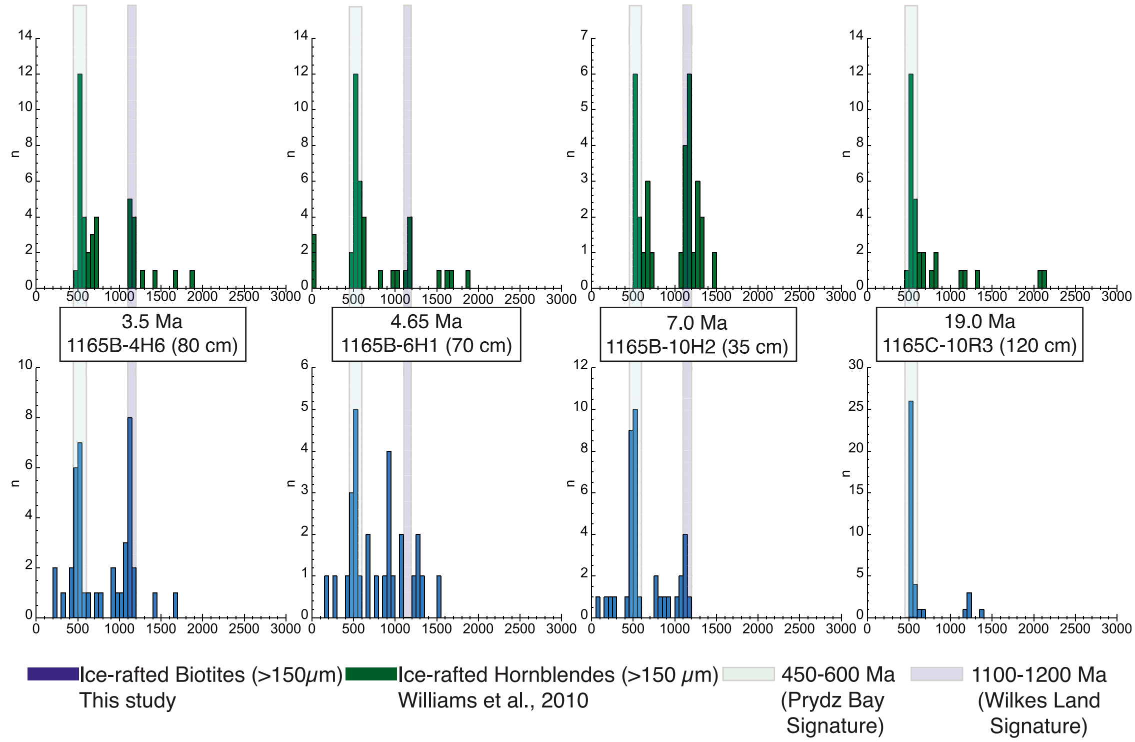


**Figure 7.** Histograms (50 Ma bins) comparing the $^{40}Ar/^{39}Ar$ hornblende ages [*Williams et al.*, 2010] and $^{40}Ar/^{39}Ar$ biotite ages from 4 ice-rafted debris-rich layers in ODP Site 1165. The blue and purple bands highlight the $^{40}Ar/^{39}Ar$ ages that fall in the 450–550 Ma and 1100–1200 Ma ranges, respectively.

#### 5.1.1.1. Ice Drainage *A*/Northern Victoria Land (~158°E to ~172°E)

[28] Ice drainage *A* is characterized by $^{40}Ar/^{39}Ar$ hornblende age populations of 0–50 Ma and 450–500 Ma, $^{40}Ar/^{39}Ar$ biotite age populations of 350–400 Ma and 450–550 Ma, and $\varepsilon_{Nd}$ values ranging from −2.7 to −10.3 (Figures 3, 4, and 7 and Table 1).

[29] A likely source for the young hornblende grains (<15 Ma) grains is the McMurdo Volcanic Group found off the coast of Victoria Land in the western Ross Sea (Figure 3a). This sector of the East Antarctic margin comprises the West Antarctic Rift System, and contains numerous volcanic rocks dated from Late Miocene through to the present [e.g., *LeMasurier and Thomson*, 1990; *Harpel et al.*, 2004; *Paulsen and Wilson*, 2007]. The population of 300–400 Ma biotites (Figure 3b) most likely reflects sourcing from the northern Bowers Terrane (~162°E, ~70.5°S), which has K-Ar dates of this age [*Adams*, 2006]. The 450–550 Ma biotite population reflects regional metamorphism associated with the Ross Orogeny [*Goodge*, 2007].

[30] Sediment cores offshore of ice drainage *A* have the most radiogenic $\varepsilon_{Nd}$ values ($\varepsilon_{Nd}$ = −2.7 to −10.1) (this study [*Roy et al.*, 2007]) (Figure 4). On-land values from 525 and 600 Ma granites on Surgeon's Island, Northern Victoria Land yield $\varepsilon_{Nd}$ = −15.6 and −16.6 [*Borg and DePaolo*, 1991]. In fact, the vast majority of the published onshore Nd isotopic compositions ($\varepsilon_{Nd}$ values of approximately −13 to −17) are much less radiogenic (Figure 4; see Table S2 for compilation of $\varepsilon_{Nd}$ values), than the values measured in the marine sediment cores. This mismatch indicates published onland Nd isotopic compositions from Sector A are not representative and that the area must be geologically more diverse. From our marine data it seems likely that mafic volcanic sources with more depleted Nd isotopic signatures (high $\varepsilon_{Nd}$) must exist next to the rather evolved granites (lower $\varepsilon_{Nd}$ [*Borg and DePaolo*, 1991]) and metasediments reported from Northern Victoria Land [*Henjes-Kunst and Schüssler*, 2003]. Indeed, substantial parts of Northern Victoria Land are reported to be comprised of mafic rocks, e.g., the Jurassic Volcanic belt of the Ferrar Group and the Precambrian meta-volcanics contained in the Nimrod and Wilson Groups [*Craddock*, 1972]. Studies on the Nd composition of the Ferrar Group show values ranging from −5 to −10 $\varepsilon_{Nd}$ [*Fleming et al.*, 1995; *Elliot et al.*, 1999].

[31] This area is an excellent example of why looking at glacially derived sediments, which integrate the overall signal of a source area, can provide a better indication of the true isotopic signal of a source area than sparse outcrop data.

#### 5.1.1.2. Ice Drainage *B*/Adélie and George V Land (Including the Wilkes Subglacial Basin) (~158°E to ~133°E)

[32] Ice Drainage *B* flows over two distinct geologic sectors, as seen in both our data and the on-land data. However, since we are presenting our new data in the context of ice drainage (and below in the context of the Wilkes sub-glacial basin), we will discuss both provenance signatures together. Ice Drainage *B* is characterized by a dominant $^{40}Ar/^{39}Ar$ hornblende age population of 1500–1800 Ma with a smaller population of 450–500 Ma, $^{40}Ar/^{39}Ar$ biotite age populations of 450–550 Ma and 1500–1800 Ma, and $\varepsilon_{Nd}$ values ranging from −12.4 to −23.6, with most values more negative than −20 (Figures 3, 4, and 6 and Table 1).

[33] The Mertz Shear zone (Figure 6) has been dated ($^{40}$Ar/$^{39}$Ar hornblende) at 1550−1500 Ma, and represents the boundary between the Terre Adélie Craton to the west and rocks associated with the Ross Orogeny to the east [*Di Vincenzo et al.*, 2007]. $^{40}$Ar/$^{39}$Ar hornblende ages from the investigated cores nicely reflect this boundary and the local on-land geology. The Terre Adélie Craton contains evidence of large-scale thermal events at ~2450 Ma and 1700 Ma [*Peucat et al.*, 1999; *Di Vincenzo et al.*, 2007; *Duclaux et al.*, 2007; *Ménot et al.*, 2007]. The least radiogenic offshore $\varepsilon_{Nd}$ values ($\varepsilon_{Nd}$ = −23.6 to −12.4) are found in the Adélie Land sector ~137°E to 145°E (this study [*Grousset et al.*, 1992; *Roy et al.*, 2007]), and agrees with known on-land $\varepsilon_{Nd}$ values (−24.9 [*Grousset et al.*, 1992])(Figure 4).

#### 5.1.1.3. Ice Drainage *C*/Wilkes Land (Including the Aurora Subglacial Basin) (~133°E to ~103°E)

[34] Ice Drainage *C* is characterized by an $^{40}$Ar/$^{39}$Ar hornblende age population of 1100–1200 Ma, an $^{40}$Ar/$^{39}$Ar biotite population of 1100–1150, and $\varepsilon_{Nd}$ values ranging from −12.3 to −16.1 (Figures 3, 4, and 7 and Table 1). ELT37–13 (Core 14) has a dominant Grenville signature and is located close to the boundary between *B* and *C*. More data would be required to evaluate whether the geological boundary extends a little to the east of the B/C drainage divide.

[35] The $^{40}$Ar/$^{39}$Ar hornblende ages are in good agreement with the results of *Roy et al.* [2007] and, though the Wilkes Land sector has few outcrops, those that do exist are consistent with the data from the marine sediment cores [*Post et al.*, 1996; *Fitzsimons*, 2000; *Post*, 2000] (Figure 3).

#### 5.1.1.4. Ice Drainage *D*/Queen Mary Land (~103°E to ~73°E)

[36] Ice Drainage *D* is characterized by only two marine sediment cores, which have $^{40}$Ar/$^{39}$Ar hornblende age populations of 1100–1250 Ma and 450–600 Ma, $^{40}$Ar/$^{39}$Arbiotite ages of 1050–1250 and 400–500 Ma, and $\varepsilon_{Nd}$ values ranging from −12.3 and −21.3 (Figures 3, 4, and 7 and Table 1). The age populations reflect the boundary between Grenville and Pan-African overprinting that occurs in Sector D [*Black et al.*, 1992; *Sheraton et al.*, 1992] (Figure 3). Marine sediment samples from Queen Mary Land are characterized by $\varepsilon_{Nd}$ values of −11.9 (this study) and −21.4 [*Basile et al.*, 1997]. On-land measurements from moraines in the Bunger Hills span a range of 14 epsilon units and are hence very poorly constrained ($\varepsilon_{Nd}$ = −9.0 and −23.0 [*Basile et al.*, 1997]).

### 5.2. Geochemical Characterization of the Wilkes and Aurora Basins

[37] Both the Wilkes and Aurora basins can be uniquely characterized based upon the combination of $^{40}$Ar/$^{39}$Ar hornblende and biotite ages and neodymium isotope measurements from marine sediments cores located off the coast proximal to each of these basins. Terrigenous material shed from the margin of East Antarctica that coincides with the Aurora sub-glacial basin (~133°E to ~105°E, also Ice Drainage *C*) is characterized by $^{40}$Ar/$^{39}$Ar hornblende and biotite ages of 1050–1200 Ma (Figure 6). These ages agree well with limited outcrops along the margin [*Post et al.*, 1996; *Fitzsimons*, 2000; *Post*, 2000].

[38] Terrigenous material shed from the margin of East Antarctica that coincides with the Wilkes sub-glacial basin (~155°E to ~135°E, also Ice Drainage *B*) also has a distinct but mixed geochemical character. The detrital $^{40}$Ar/$^{39}$Ar hornblende and biotite ages have a dominant population of 1500–1800 Ma (Figure 6), which is consistent with on-land ages [*Peucat et al.*, 1999; *Di Vincenzo et al.*, 2007; *Ménot et al.*, 2007]. In addition to this age population, there is also a significant 400–500 Ma population, mainly in the biotites. Thus, the signature for the Wilkes Basin consists of two $^{40}$Ar/$^{39}$Ar age populations: 1500–1800 Ma for both biotites and hornblendes, and 450–500 Ma, dominated mainly by biotite ages but including some hornblende ages.

[39] Given the physical characteristics of both of these basins, i.e., that the majority of the elevation lies more than 500 m below sea level and that they contain reverse bed slopes (where the bed deepens inland), these areas might serve as zones of weakness to the East Antarctic ice sheet. *Schoof* [2007] showed that the flux of ice at the grounding line increases as the depth of the grounding line below sea level increases. Where the grounding line rests on a reverse slope bed, retreat of the grounding line can set off a cycle of increased ice-discharge and further retreat, which will continue until a new equilibrium can be reached. It is plausible that such grounding line retreat and ice-discharge occurred on the Wilkes and Aurora subglacial basins in the past. An important outcome of this work is recognition that sediments being shed from the outlets of either of the basins are geochemically distinguishable from the other. This lays the foundations for future studies investigating the role of these basins in the evolution of the EAIS.

### 5.3. Comparison of IRD Tracers

#### 5.3.1. Individual Detrital Minerals

#### 5.3.1.1. $^{40}$Ar/$^{39}$Ar Hornblende and Biotite Ages

[40] $^{40}$Ar/$^{39}$Ar biotite ages from the >150 $\mu$m and 63–150 $\mu$m size fractions agree well with one another and can be treated as one population (Table 1 and Figure 5). Because the $^{40}$Ar/$^{39}$Ar biotite ages from these size fractions are in good agreement with each other, we restrict this part of the discussion to a comparison of the $^{40}$Ar/$^{39}$Ar hornblende ages to the biotite ages. $^{40}$Ar/$^{39}$Ar biotite ages are mostly consistent with, although slightly younger than, the $^{40}$Ar/$^{39}$Ar hornblende ages (Figure 6 and Table 1). Given their respective closure temperatures of ~300°C and ~500°C, this observation indicates moderately fast cooling immediately following the most recent tectonothermal event.

[41] We have calculated robust median ages for each of the $^{40}$Ar/$^{39}$Ar age populations from all marine sediment cores in this study using ISOPLOT/Ex Program v. 3.00 (an Excel-powered program that allows for manipulation of radiogenic isotope data [*Ludwig*, 2003]), in order to more closely compare the ages of these two thermochronometers (Table 2). As can be seen from Table 2, the age difference between the $^{40}$Ar/$^{39}$Ar hornblende and $^{40}$Ar/$^{39}$Ar biotite ages is quite small at most sites (1 to 108 Myr), with almost all age differences less than 80 Myr.

[42] The $^{40}$Ar/$^{39}$Ar ages of individual minerals present a straightforward characterization of the East Antarctic margin between the Ross Sea and Prydz Bay (Figure 3), as discussed in section 5.1. There is little overlap in age populations, and the data we have measured in the marine sediment cores match well with available on-land measurements (Figure 3). Importantly, this agreement in $^{40}$Ar/$^{39}$Ar ages indicates that where there is little or no outcrop data, the

**Table 2.** Robust Median Ages of Hornblende and Biotite $^{40}Ar/^{39}Ar$ Age Populations by Marine Sediment Core[a]

| | | $^{40}Ar/^{39}Ar$ Hornblende and Biotite Ages | | | | | | | | | |
|---|---|---|---|---|---|---|---|---|---|---|---|
| | | Hornblendes | | | | | Biotites | | | | |
| Core | Site | Grains | Robust Median Age (Ma) | ± | Error (%) | Confidence Interval | Grains | Robust Median Age (Ma) | ± | Error (%) | Confidence Interval |
| 7 | DF80–34 | 9 | 8.8 | +1.9/−5.8 | 44 | 96.1 | - | - | - | - | - |
| | | - | - | - | - | - | 7 | 370 | +25/−67 | 12 | 98.4 |
| | | | 492 | +9.5/−13 | 2.3 | 97.9 | 19 | 491 | +20/−14 | 3.4 | 93.6 |
| 5 | DF80–35 | 14 | 7.6 | +2.8/−7.5 | 41 | 94.3 | - | - | - | - | - |
| | | - | - | - | - | - | 19 | 371.1 | +4/−9.9 | 1.9 | 93.6 |
| 6 | DF80–20 | 5 | 373 | 13/−10 | 19 | 93.8 | 22 | 368.2 | +2.2/−2.6 | 0.65 | 94.8 |
| | | - | - | - | - | - | 7 | 473 | +21/−61 | 8.6 | 98.4 |
| 9 | DF79–47 | 18 | 508.6 | +9.9/−18 | 2.8 | 96.9 | 8 | 491 | +45/−54 | 10 | 93 |
| | | 17 | 1530 | +17/−6 | 7.5 | 95.1 | - | - | - | - | - |
| 11 | JPC11 2305 | 13 | 1651 | +79/−40 | 6.7 | 97.8 | 14 | 1635 | +48/−27 | 2.3 | 94.3 |
| 11 | JPC11 2370 | 31 | 1690 | +63/−39 | 3 | 97 | 15 | 1619 | +22/−20 | 1.5 | 96.5 |
| 12 | ELT37–09 | - | - | - | - | - | 35 | 494 | +10/−13 | 2.5 | 95 |
| | | 33 | 1693 | +68/−34 | 3 | 95 | 14 | 1585 | +59/−23 | 2.6 | 94.3 |
| 14 | ELT37–13 | 41 | 1162 | +32/−31 | 2.7 | 95 | 26 | 1117.3 | +4.2/−8.7 | 0.57 | 95 |
| 15 | ELT37–16 | 35 | 1165 | 12 | 1.1 | 95 | 53 | 1123.1 | +15/−17.8 | 1 | 95 |
| 20 | ELT49–30 | - | - | - | - | - | 12 | 471 | +24/−35 | 6 | 96.1 |
| | | 27 | 1164.5 | +8.2/−8.7 | 0.73 | 95 | 14 | 1088 | +24/−22 | 2.1 | 94.5 |

[a]Robust median age of hornblende and biotite $^{40}Ar/^{39}Ar$ age populations by marine sediment core. Robust median ages were calculated over the following age intervals, if they exist in the total population: 0–50 Ma, 300–400 Ma, 400–600 Ma, 900–1400 Ma, 1400–2000 Ma.

marine sediment $^{40}Ar/^{39}Ar$ provide robust information on the adjacent coast.

#### 5.3.1.2. Decoupling of $^{40}Ar/^{39}Ar$ Hornblende and Biotite Ages

[43] While the $^{40}Ar/^{39}Ar$ hornblende and biotite age populations from the marine sediment cores generally agree with one another, differences may provide information about the composition and history of the onshore terranes. Two apparent mechanisms could serve to decouple the $^{40}Ar/^{39}Ar$ hornblende and $^{40}Ar/^{39}Ar$ biotite ages, resulting in different populations of ages between the two minerals. First, there is a lithological bias, as hornblendes tend to form in intermediate to mafic rocks, while biotites tend to form in felsic rocks. Both minerals are found in a range of metamorphic rocks. Thus, if a source area has a tendency toward the lithology favored by one mineral over the other, age populations would be biased to that source. A second mechanism for decoupling the $^{40}Ar/^{39}Ar$ ages is low-grade, greenschist facies metamorphism, which could re-set $^{40}Ar/^{39}Ar$ biotite ages (closure temperature of ~300°C) without re-setting the hornblende ages (closure temperature of ~500°C).

[44] An apparent decoupling between the $^{40}Ar/^{39}Ar$ hornblende and biotite ages is found in several cores (Core 12: ELT37–09 (140–144 cm), Core 9: DF79–47 (563–567 cm), and Cores 5, 6 and 7 (Figure 4 and Table 1). First, the distribution of $^{40}Ar/^{39}Ar$ biotite ages in Core 12 (ELT37–09, 140–144 cm) reveals an age population of 450–550 Ma that is represented by only a few hornblendes ages; the dominant hornblende population for this sample is 1550–1800 Ma. To explore whether this ~500 Ma biotite age population is evidence of an ice-rafting event delivering ~500 Ma biotite grains from sources far from the core site (e.g., east of ~146°E), or alternatively, a compositional bias in the two age provinces, we analyzed two other terrigenous-rich layers in Core ELT37–09 (92–93 cm and 137–139 cm). We found that the ~500 Ma biotite population exists in all three layers (Table 1), indicating that either this is a relatively local, previously unidentified, source or that this site is routinely the locus of deposition of similar far-traveled icebergs. We favor the local source due to the similar age distributions in the three samples. While no $^{40}Ar/^{39}Ar$ biotite ages of ~500 Ma have been reported west of the Mertz Glacier (~145°E; Figure 6) [*Duclaux et al.*, 2008], we speculate that the $^{40}Ar/^{39}Ar$ biotite ages may reflect the ~500 Ma greenschist metamorphism recorded at Cape Denison and Cape Hunter (Adélie Land), described by *Stüwe and Oliver* [1989]. This type of metamorphism could potentially reset biotite ages, without resetting amphibole ages. Furthermore the greenschist metamorphism at Cape Denison and Cape Hunter (~142°E to ~143°E) (*Stüwe and Oliver*'s [1989] M3 event) is expressed as assemblages primarily of epidote, lawsonite, biotite, chlorite and white mica, with very little hornblende.

[45] The second example of contrast comes from Core 9 (DF79–47, 563–567 cm) where both biotites and hornblendes show a ~500 Ma age population consistent with on-land geology, but prominent ages of >1500 Ma consistent with the age of the Mertz Shear Zone (MSZ) [*Di Vincenzo et al.*, 2007] are found in the hornblendes, but not in the biotites. As with the case from ELT37–09, this is likely the result of a compositional bias, as the lithology of the rocks to the east of the Mertz Glacier that show Ross Orogen ages are biotite granites, granitoids and metasediments [*Di Vincenzo et al.*, 2007; *Duclaux et al.*, 2007], while the rocks to the west of the Mertz Glacier are a mixture of high-grade metamorphic rocks, such as amphibole-rich granulites, migmatites and various gneisses [*Duclaux et al.*, 2007]. It is important to note that Core 9 is ~100 km to the east of where the MSZ outcrops (Figure 6), and that the coastal current flows from east to west, making it unlikely that grains would be delivered to Core 9 from this location. However, geophysical interpretations show that the MSZ extends into the continent to the southeast [*Ferraccioli et al.*, 2009] and so material may be sourced from the MSZ under the ice sheet, and to the east of where it outcrops.

[46] In a third example of contrast, the difference between hornblende and biotite $^{40}Ar/^{39}Ar$ age populations in Cores 5,

**Table 3.** Comparison of Robust Median Ross Orogen and Pan-African Orogen Ages[a]

| | $^{40}Ar/^{39}Ar$ Hornblende and Biotite Ages | | | | | | | | | |
|---|---|---|---|---|---|---|---|---|---|---|
| | $^{40}Ar/^{39}Ar$ Hornblende Ages | | | | | $^{40}Ar/^{39}Ar$ Biotite Ages | | | | |
| Orogeny | Grains | Robust Median Age (Ma) | ± | Error (%) | Confidence Interval | Grains | Robust Median Age (Ma) | ± | Error (%) | Confidence Interval |
| Ross Orogeny | 55 | 492.3 | +5/−6.9 | 1.2 | 95 | 85 | 492.1 | +2.7/−7.0 | 0.98 | 95 |
| Pan-African | 42 | 517 | +12/−6.8 | 1.9 | 95 | 12 | 471 | +24/−33 | 6 | 96.1 |

[a]Comparison of Ross Orogen (450–550 Ma) and Pan-African (450–600 Ma) robust median ages. Robust median ages calculated from hornblende and biotite data falling in the 400–600 Ma range. Hornblende ages from cores 1–9 and biotites from cores 1–12 were used to calculate the Ross Orogen ages. Hornblendes from cores 19–21 and biotites from core 20 were used to calculate the Pan-African ages.

6, and 7, appears to be the result of compositional bias, e.g., more mafic rocks contain hornblendes and not biotites, whereas more felsic rocks tend to contain more biotites than hornblendes. While hornblendes mostly show ages reflecting the Ross Orogen and young volcanics from the western Ross Sea, the biotites show dominant ages in the 300–400 Ma range, reflecting the Bowers Terrane of Northern Victoria Land.

#### 5.3.1.3. $^{40}Ar/^{39}Ar$ Biotites as an IRD Tracer at ODP Site 1165

[47] The new $^{40}Ar/^{39}Ar$ biotite ages from ODP Site 1165 are consistent with the $^{40}Ar/^{39}Ar$ hornblende ages from *Williams et al.* [2010] (Figure 7), bearing in mind the lower closure temperature for biotite. Each of the four layers from Site 1165 contains a biotite age population of 450–550 Ma compared to $^{40}Ar/^{39}Ar$ hornblende ages of 450–600 Ma [*Williams et al.*, 2010]. *Williams et al.* [2010] attributed these ages to the local Prydz Bay area based upon both onshore evidence [*Tong et al.*, 1998; *Phillips et al.*, 2007; *Wilson et al.*, 2007] and evidence from $^{40}Ar/^{39}Ar$ measurements on detrital hornblendes from marine sediment core samples [*Roy et al.*, 2007; *van de Flierdt et al.*, 2008], all of which show a dominant ~500 Ma age. These $^{40}Ar/^{39}Ar$ biotite ages are also consistent with the peak $^{40}Ar/^{39}Ar$ biotite age (~502 Ma) measured from glacial-marine sediments in ODP Site 1166, located in Prydz Bay [*van de Flierdt et al.*, 2008], as well as onshore evidence [*Tong et al.*, 2002].

[48] The three layers from ODP Site 1165 containing far-traveled hornblende grains from Wilkes Land (with a characteristic $^{40}Ar/^{39}Ar$ age of 1100–1200 Ma) also contain biotite $^{40}Ar/^{39}Ar$ ages in the 1100–1200 Ma range. This typical Grenvillian age range is absent from rocks exposed in the Prydz Bay area and also has not been found in modern sediments [see *Williams et al.*, 2010].

[49] These results indicate that the added use of $^{40}Ar/^{39}Ar$ biotite ages as a complement to $^{40}Ar/^{39}Ar$ hornblende ages for tracing IRD in the Southern Ocean is a useful approach, for two reasons. First, by analyzing both hornblendes and biotites, we reduce any lithological bias that might occur by analyzing only hornblendes, and second, as we can measure $^{40}Ar/^{39}Ar$ biotite ages in the 63–150 $\mu$m fraction, this may provide the only viable option in samples with very low IRD concentrations.

#### 5.3.2. The $\varepsilon_{Nd}$ Values as a Tracer of an Integrated Erosional Signal

[50] The $\varepsilon_{Nd}$ values also provide characterization of the 4 drainage sectors. However, based on all of the $\varepsilon_{Nd}$ values from this margin of East Antarctica (our new data, previous marine sediment core studies and the on-land $\varepsilon_{Nd}$ values, summarized in Figure 4) it is apparent that while each of the 4 sectors has a distinct range of values, there is some overlap between sectors. For example, $\varepsilon_{Nd}$ values from marine sediment samples that characterize both ice-drainage *B* and *C* have $\varepsilon_{Nd}$ values that fall in the −12 to −15 range. In addition, some on-land outcrop values do not agree with the values measured in marine sediment cores; a discrepancy that is the result of (1) the control that lithology has on a measured $\varepsilon_{Nd}$ value (for example, mafic lithologies are expected to have more radiogenic (less negative) values than felsic lithologies) and (2) the fact that the $\varepsilon_{Nd}$ value measured in the marine sediment cores represents an average of the proximal geology that is not necessarily evenly sampled.

[51] It is interesting that the $\varepsilon_{Nd}$ values measured in the marine sediment cores allow for a better division of this margin of East Antarctica than the on-land values. For example, in ice drainage *A* the majority of on-land $\varepsilon_{Nd}$ values fall mostly in the −13 to −17 range, comparable to values obtained in the glacial-marine sediments in sectors *B* and *C*, while the marine sediment core $\varepsilon_{Nd}$ values fall in the −3 to −10 range. This highlights an advantage of characterizing source areas by looking at proximal marine sediments, as these reveal a true average of the erosion products being shed from under the ice sheet, and overcome the sampling bias from on-land studies.

### 5.4. Pan-African and Ross Orogen Ages and Cooling History

[52] The $^{40}Ar/^{39}Ar$ ages of the Pan-African orogeny (Prydz Bay, 600–500 Ma) and Ross Orogeny (Northern Victoria Land, 550–450 Ma) are known from relatively few onshore exposures, and the larger amount of offshore data present the opportunity to date the cooling phases of these orogenies more precisely. Additionally, information about the cooling rate can be determined from the difference in $^{40}Ar/^{39}Ar$ ages between hornblende (set at ~500°C) and biotite (set at ~300°C). In order to see if our data show distinguishable age peaks between sediments affected by either the Pan-African (650–500 Ma) or Ross (550–450 Ma) orogenies, we have calculated the robust median age of hornblende and biotite $^{40}Ar/^{39}Ar$ ages using the $^{40}Ar/^{39}Ar$ ages of grains from cores proximal to those areas of East Antarctica affected by Ross and Pan-African overprinting (Table 3). Ages reflecting the Ross Orogeny have robust median ages of 492.3 Ma (+5/−6.9 Ma) (hornblendes) and 492.1 Ma (+2.7/−7.0 Ma) (biotites), while ages reflecting the Pan-African orogeny have

robust median ages of 517 Ma (+12/−6.8 Ma) (hornblendes) and 471 Ma (+23/−33 Ma) (biotites). Thus, while the hornblende $^{40}Ar/^{39}Ar$ ages reflecting the Pan-African orogeny are older than those reflecting the Ross orogeny, the opposite is true for the $^{40}Ar/^{39}Ar$ biotite ages. There is very little age difference between $^{40}Ar/^{39}Ar$ hornblende and biotite ages for the Ross orogeny, while there is nearly a 50 million year difference for the Pan-African Orogeny, indicating rapid cooling following the Ross Orogeny, and much slower cooling following the Pan-African. Using our peak age calculations, and assuming closure temperatures for $^{40}Ar/^{39}Ar$ hornblende (~500°C) and $^{40}Ar/^{39}Ar$ biotite (~300°C) ages, the implied cooling rates for the Ross and Pan-African orogenies would be incredibly fast (due nearly identical $^{40}Ar/^{39}Ar$ hornblende and biotite ages), with ~ 4–5°C $Myr^{-1}$, respectively.

[53] Our data are consistent with previous studies, in that the Pan-African orogeny is slightly older than the Ross Orogeny. The onset of the Pan-African orogeny in the western Prydz Bay/Queen Mary Land area predated the onset of the Ross Orogeny, starting around 600 Ma [*Veevers*, 2003, 2004], nearing completion around 500 Ma, and with peak ages of 550–500 Ma [*Meert*, 2003], based mostly on zircon U-Pb data. Subduction associated with the Ross Orogeny commenced ~ 550 Ma forming a convergent margin that lasted until 450 Ma [*Goodge*, 1997]. Ross Orogen ages found on-land in Oates Land and Northern Victoria land are younger than 530 Ma [*Adams*, 2006; *Di Vincenzo et al.*, 2007; *Goodge*, 2007], with peak Ross Orogen ages of 500 Ma [*Goodge*, 1997, 2007].

[54] Our interpreted rapid cooling rate following the Ross Orogeny is compatible with some previous studies. While cooling rates from across Northern Victoria Land (NVL) range from 18° to 30°$Myr^{-1}$ [*Goodge and Dallmeyer*, 1996; *Schüssler et al.*, 1999], both *Di Vincenzo et al.* [1997] and *Palmeri et al.* [2003] argue for very fast cooling in the NVL area based on overlapping ages in high-temperature thermochronometers (consistent with our near-identical $^{40}Ar/^{39}Ar$ hornblende and biotite age peaks).

[55] Cooling rates for the Prydz Bay area also show a range. *Fitzsimons et al.* [1997] present data that supports a multistage cooling history from the eastern Prydz Bay area with initial cooling rates of 20°$myr^{-1}$ followed by cooling rates of 5°$myr^{-1}$. However, they also show that an average cooling rate of ~10°$myr^{-1}$ fits their data equally well. *Zhao et al.* [1997] inferred cooling rates of nearly 40°C$myr^{-1}$ from the same area. Slower cooling rates (3°$myr^{-1}$) are reported from the northern Prince Charles mountains (western Prydz Bay), but these appear to be restricted to this particular area [*Zhao et al.*, 2003]. Thus, it would appear that our ~4°–5°$myr^{-1}$ cooling rate is anomalously low compared to measurements from outcrops. More data, and particularly more biotite data, from cores along this margin would provide more information. Using pairs of hornblende and biotite ages from pebbles and cobbles found in marine sediment cores along the margin would also offer more information as different sources of the two grain types can be excluded when derived from the same pebble.

[56] While our data cannot definitively elucidate cooling rates for either of the orogenies at this point, it shows that the presented approach is a plausible method for estimating average cooling rates and exhumation histories for parts of Antarctica that are ice-covered, and thus inaccessible to direct study. Further studies should aim for a larger number of detrital thermochronometers in order to better constrain these rates.

## 6. Conclusions

[57] We have performed an extensive survey of the $^{40}Ar/^{39}Ar$ ages of detrital hornblende and biotite grains in ice-rafted debris and Nd isotopes on the bulk < 63 $\mu$m size fraction from marine sediment cores along the margin of East Antarctica from 94°E to 165°E. We measured an average of 78 (minimum of 29, maximum of 119) $^{40}Ar/^{39}Ar$ ages from 8 marine sediment cores for a total of 626 analyses. This large number of analyses provides robust statistics to support the following conclusions:

[58] 1. The $^{40}Ar/^{39}Ar$ ages and neodymium isotope results obtained from marine sediment cores agree well with sparse outcrops and other marine sediment core data, both serving to better constrain our knowledge of provenance areas around Antarctica that could have been the loci of iceberg calving and/or fine sediment discharge in the past. Our data improves the geological characterization for East Antarctic IRD source areas by quadrupling the number of $^{40}Ar/^{39}Ar$ analyses from detrital minerals and adding eight new Nd measurements of the bulk < 63 $\mu$m fraction from marine sediment cores along this margin, including areas that are ice-covered. With the Nd data, we have shown the importance of characterizing source areas around East Antarctica by looking at proximal glacial-marine sediments, as these measurements provide the integrated isotopic composition of the source areas. With the $^{40}Ar/^{39}Ar$ hornblende and biotite data, we have shown the advantage of measuring ages on the individual minerals, as such measurements allow for representation of all end-members (in contrast, bulk geochemical analyses are a mixture of the end-members).

[59] 2. Sediments shed from along the continental margin where the Wilkes and Aurora sub-glacial basins terminate can be distinguished by a combination of their $^{40}Ar/^{39}Ar$ hornblende and biotite ages, in addition to the Nd isotopic composition of the bulk < 63 $\mu$m fraction. The Wilkes Basin is characterized by $^{40}Ar/^{39}Ar$ hornblende and biotite ages of 1500–1800 Ma, with a significant biotite population of 450–550 Ma, and unradiogenic $\varepsilon_{Nd}$ values (mostly less than −16.1). The Aurora Basin is characterized by $^{40}Ar/^{39}Ar$ hornblende and biotite ages of 1100–1200 Ma, and more radiogenic $\varepsilon_{Nd}$ values of −11.7 to −14.9. The $\varepsilon_{Nd}$ values for both basins show some overlap, with the exception of the very unradiogenic values off the coast of Adélie Land that characterize part of the Wilkes Basin. The Aurora Basin is characterized by distinct Grenvillian $^{40}Ar/^{39}Ar$ ages of 1100 to 1200 Ma. The Wilkes basin drains an area affected by multiple tectonothermal events as reflected in multiple age populations (Ross Orogeny ages of ~500 Ma and Adélie Land ages of 1500 to 1700 Ma). Our new data lend further support to the suggested instability of East Antarctic sub-glacial basins during times of past warmth [*Williams et al.*, 2010] and should prove important to future provenance studies, aiming to improve our understanding of EAIS evolution and the role of the Wilkes and Aurora sub-glacial basins in ice instabilities in the past.

[60] 3. We have characterized each of the four ice drainage divides (*A – D*) [*Vaughan et al.*, 1999] that terminate along this margin of East Antarctica using a combination of $^{40}Ar/^{39}Ar$ hornblende and biotite ages of individual grains and bulk $\varepsilon_{Nd}$ of the < 63 $\mu$m fraction. Drainages *A* and *C* show a unique geochemical signature based upon these provenance tools. Drainages *B* and *D* have a mixed signal as they drain parts of the EAIS that cross major geologic boundaries; Drainage *B* drains over the divide between rocks affected by Ross orogen overprinting and much older thermal events, while Drainage *D* drains over the boundary between Pan-African (450–600 Ma) and Grenville (1000–1300 Ma) overprinting.

[61] 4. The use of $^{40}Ar/^{39}Ar$ dating of detrital hornblendes and biotites in marine sediments is a robust way to determine the provenance of ice-rafted debris around the East Antarctic perimeter. Given that both minerals are major rock-forming minerals it is reasonable to expect that they will be constituents in IRD; however this is dependent upon the source lithologies contributing to the sediment sample. $^{40}Ar/^{39}Ar$ ages of hornblendes can effectively be treated as crystallization ages (amphibolite-grade metamorphism), as the closure temperature for this system is ~500°, thus allowing for inferences about the geology underlying the ice sheet to be made, while $^{40}Ar/^{39}Ar$ ages in biotites record cooling below ~300°C, and thus are more susceptible to re-setting. Based on our data it is clear that the $^{40}Ar/^{39}Ar$ biotite ages can serve as a provenance tracer for IRD around East Antarctica.

[62] **Acknowledgments.** This research was funded by NSF grants ANT 09–44489, ANT 08–38729, and ANT 05–38580. T.v.D.F. acknowledges funding by NERC NE/H014144/1 and Marie Curie IRG 230828. S. Brachfeld acknowledges NSF grant ANT 03–48274. The flux fusion setup used for the Nd isotopes was funded by the Climate Center at Lamont (T.v.D.F. and Franzese). We thank Florida State University's Antarctic Marine Geology Repository for providing the piston and jumbo piston core samples, and especially C. Sjunneskog for help with sample age determinations, and IODP for providing the samples from Leg 188 ODP Site 1165. C. Doherty, G. Mesko, L. Bolge, E. Palmer and S. Cox are gratefully acknowledged for their help with sample processing. We also thank two anonymous reviewers for constructive comments on this manuscript.

## References


Adams, C. J. (2006), Style of uplift of Paleozoic terranes in northern Victoria Land, Antarctica: Evidence from K-Ar Age Patterns, in *Antarctica: Contributions to Global Earth Sciences*, edited by D. K. Futterer et al., pp. 205–214, Springer, Berlin.

Alley, R. B., T. K. Dupont, B. R. Parizek, S. Anandakrishnan, D. E. Lawson, G. J. Larson, and E. B. Evenson (2006), Outburst flooding and the initiation of ice-stream surges in response to climatic cooling: A hypothesis, *Geomorphology*, *75*, 76–89.

Bamber, J. L., D. G. Vaughan, and I. Joughin (2000), Widespread complex flow in the interior of the Antarctic ice sheet, *Science*, *287*, 1248–1250, doi:10.1126/science.287.5456.1248.

Basile, I., F. E. Grousset, M. Revel, J. R. Petit, P. E. Biscaye, and N. I. Barkov (1997), Patagonian origin of glacial dust deposited in East Antarctica (Vostok and Dome C) during glacial stages 2,4 and 6, *Earth Planet. Sci. Lett.*, *146*, 573–589, doi:10.1016/S0012-821X(96)00255-5.

Bell, R. E. (2008), The role of subglacial water in ice-sheet mass balance, *Nature*, *1*, 297–304.

Billups, K., and D. P. Schrag (2002), Paleotemperatures and ice volume of the past 27 Myr revisited with paired Mg/Ca and $^{18}O/^{16}O$ measurements on benthic foraminifera, *Paleoceanography*, *17*(1), 1003, doi:10.1029/2000PA000567.

Billups, K., and D. P. Schrag (2003), Application of benthic foraminiferal Mg/Ca ratios to questions of Cenozoic climate change, *Earth Planet. Sci. Lett.*, *209*, 181–195, doi:10.1016/S0012-821X(03)00067-0.

Black, L. P., J. W. Sheraton, R. J. Tingey, and M. T. McCulloch (1992), New U-Pb zircon ages from the Denman Glacier area, East Antarctica, and their significance for Gondwana reconstruction, *Antarct. Sci.*, *4*, 447–460, doi:10.1017/S095410209200066X.

Boger, S. D., C. J. Carson, C. L. J. Wilson, and C. M. Fanning (2000), Neoproterozoic deformation in the Radok Lake region of the northern Prince Charles Mountains, East Antarctica; evidence for a single protracted orogenic event, *Precambrian Res.*, *104*, 1–24, doi:10.1016/S0301-9268(00)00079-6.

Borg, S. G., and D. J. DePaolo (1991), A tectonic model of the Antarctic Gondwana margin with implications for southeastern Australia: Isotopic and geochemical evidence, *Tectonophysics*, *196*, 339–358, doi:10.1016/0040-1951(91)90329-Q.

Borg, S. G., E. Stump, B. W. Chappell, M. T. McCulloch, D. Wyborn, R. L. Armstrong, and J. R. Holloway (1987), Granitoids of northern Victoria Land, Antarctica: Implications of chemical and isotopic variations to regional crustal structure and tectonics, *Am. J. Sci.*, *287*, 127–169, doi:10.2475/ajs.287.2.127.

Brachfeld, S. A., S. R. Hemming, T. van de Flierdt, S. L. Goldstein, M. Roy, T. Williams, and M. Rosig (2007), Integrated provenance characteristics of glacial-marine sediment from East and West Antarctica, in *Antarctica: A Keystone in a Changing World: Proceedings of the 10th International Symposium on Antarctic Earth Sciences, Santa Barbara, California, August 26 to September 1, 2007*, edited by A. K. Cooper et al., p. 3, Natl. Acad., Washington, D. C.

Carson, C. J., S. D. Boger, C. M. Fanning, C. J. L. Wilson, and D. E. Thost (2000), SHRIMP U-Pb geochronology from Mount Kirby, northern Prince Charles Mountains, East Antarctica, *Antarct. Sci.*, *12*, 429–442, doi:10.1017/S0954102000000523.

Craddock, C. (1972), *Geologic Map of Antarctica*, Am. Geogr. Soc., New York, NY.

DeConto, R. M., and D. Pollard (2003), Rapid Cenozoic Glaciation of Antarctica induced by declining atmospheric $CO_2$, *Nature*, *421*, 245–249, doi:10.1038/nature01290.

Di Vincenzo, G., R. Palmeri, F. Talarico, P. A. M. Andriessen, and C. A. Ricci (1997), Petrology and geochronology of eclogites from the Lanterman Range, Antarctica, *J. Petrol.*, *38*(10), 1391–1417, doi:10.1093/petrology/38.10.1391.

Di Vincenzo, G., F. Talarico, and G. Kleinschmidt (2007), An $^{40}Ar/^{39}Ar$ investigation of the Mertz Glacier area (George V Land, Antarctica): Implications for the Ross Orogen-East Antarctic craton relationship and Gondwana reconstructions, *Precambrian Res.*, *152*, 93–118, doi:10.1016/j.precamres.2006.10.002.

Drewry, D. J. (Ed.) (1983), *Antarctica: Glaciological and Geophysical Folio*, Scott Polar Res. Inst., Cambridge, U. K.

Duclaux, G., Y. Rolland, G. Ruffet, R. P. Ménot, S. Guillot, J. J. Peucat, and J. Bascou (2007), Superposition of Neoarchean and Paleoproterozoic tectonics in the Terre Adélie Craton (East Antarctica): Evidence from Th-U-Pb ages on monazite and Ar-Ar ages, in *Antarctica: A Keystone in a Changing World: Proceedings of the 10th International Symposium on Antarctic Earth Sciences, Santa Barbara, California, August 26 to September 1, 2007*, edited by A. K. Cooper et al., pp. 1–4, Natl. Acad., Washington, D. C.

Duclaux, G., Y. Rolland, G. Ruffet, R.-P. Ménot, S. Guillot, J.-J. Peucat, M. Fanning, P. Rey, and A. Pêcher (2008), Superimposed Neoarchaean and Paleoproterozoic tectonics in the Terre Adélie Craton (East Antarctica): Evidence from Th–U–Pb ages on monazite and $^{40}Ar/^{39}Ar$ ages, *Precambrian Res.*, *167*, 316–338, doi:10.1016/j.precamres.2008.09.009.

Elliot, D. H., T. H. Fleming, P. R. Kyle, and K. A. Foland (1999), Long-distance transport of magmas in the Jurassic Ferrar Large Igneous Province, Antarctica, *Earth Planet. Sci. Lett.*, *167*, 89–104, doi:10.1016/S0012-821X(99)00023-0.

Erlingsson, U. (1994), The 'Captured Ice Shelf' hypothesis and its applicability to the Weichselian glaciation, *Geogr. Ann. Ser. A*, *76*(1–2), 1–12, doi:10.2307/521315.

Escutia, C., L. De Santis, F. Donda, R. B. Dunbar, A. K. Cooper, G. Brancolini, and S. L. Eittreim (2005), Cenozoic ice sheet history from East Antarctic Wilkes Land continental margin sediments, *Global Planet. Change*, *45*, 51–81, doi:10.1016/j.gloplacha.2004.09.010.

Farmer, G. L., D. C. Barber, and J. T. Andrews (2003), Provenance of Late Quaternary ice proximal sediments in the North Atlantic: Nd, Sr and Pb isotopic evidence, *Earth Planet. Sci. Lett.*, *209*, 227–243, doi:10.1016/S0012-821X(03)00068-2.

Ferraccioli, F., E. Armadillo, T. Jordan, E. Bozzo, and H. Corr (2009), Aeromagnetic exploration over the East Antarctic ice sheet: A new view of the Wilkes Subglacial Basin, *Tectonophysics*, *478*, 62–77, doi:10.1016/j.tecto.2009.03.013.

Fitzsimons, I. C. W. (2000), Grenville-age basement provinces in East Antarctica: Evidence for three separate collisional origins, *Geology*, *28*(10), 879–882, doi:10.1130/0091-7613(2000)28 < 879:GBPIEA > 2.0.CO;2.

Fitzsimons, I. C. W., P. D. Kinny, and S. L. Harley (1997), Two stages of zircon and monazite growth in anatectic leucogneiss: SHRIMP constraints on the duration and intensity of Pan-African metamorphism in Prydz Bay, East Antarctica, *Terra Nova*, *9*, 47–51, doi:10.1046/j.1365-3121.1997.d01-8.x.

Fleming, T. H., K. A. Foland, and D. H. Elliot (1995), Isotopic and chemical constraints on the crustal evolution and source signature of Ferrar magmas, north Victoria Land, Antarctica, *Contrib. Mineral. Petrol.*, *121*(3), 217–236, doi:10.1007/BF02688238.

Flower, B. P., and J. P. Kennett (1994), The middle Miocene climatic transition: East Antarctic ice sheet development, deep ocean circulation and global carbon cycling, *Palaeogeogr. Palaeoclimatol. Palaeoecol.*, *108*, 537–555, doi:10.1016/0031-0182(94)90251-8.

Giovinetto, M. B., and C. R. Bentley (1985), Surface balance in ice drainage systems of Antarctica, *Antarct. J. U. S.*, *20*, 6–13.

Goodge, J. W. (1997), Latest Neoproterozoic basin inversion of the Beardmore Group, central Transantarctic Mountains, Antarctica, *Tectonics*, *16*(4), 682–701, doi:10.1029/97TC01417.

Goodge, J. W. (2007), Metamorphism in the Ross orogen and its bearing on Gondwana margin tectonics, in *Convergent Margin Terranes and Associated Regions: A Tribute to W.G. Erns*, edited by M. Cloos et al., *Geol. Soc. Am. Spec. Pap.*, *419*, 185–203.

Goodge, J. W., and D. R. Dallmeyer (1996), Contrasting thermal evolution within the Ross orogen, Antarctica: Evidence from mineral $^{40}Ar/^{39}Ar$ Ages, *J. Geol.*, *104*, 435–458, doi:10.1086/629838.

Grousset, F. E., P. E. Biscaye, M. Revel, J.-R. Petit, K. Pye, S. Joussaume, and J. Jouzel (1992), Antarctic (Dome C) ice-core dust at 18 k.y. B.P.: Isotopic constraints on origins, *Earth Planet. Sci. Lett.*, *111*, 175–182, doi:10.1016/0012-821X(92)90177-W.

Grousset, F. E., L. Labeyrie, J. A. Sinko, M. Cremer, G. Bond, J. Duprat, E. Cortijo, and S. Huon (1993), Patterns of ice-rafted detritus in the glacial North Atlantic (40–55°N), *Paleoceanography*, *8*(2), 175–192, doi:10.1029/92PA02923.

Gwiazda, R. H., S. R. Hemming, W. S. Broecker, T. Onsttot, and C. Mueller (1996), Evidence from $^{40}Ar/^{39}Ar$ ages for a Churchill Province source of ice-rafted amphiboles in Heinrich layer 2, *J. Glaciol.*, *42*, 440–446.

Hambrey, M. J., and B. McKelvey (2000), Major Neogene fluctuations of the East Antarctic ice sheet: Stratigraphic evidence from the Lambert Glacier region, *Geology*, *28*, 887–890, doi:10.1130/0091-7613(2000)28<887:MNFOTE>2.0.CO;2.

Harpel, C. J., P. R. Kyle, R. P. Esser, W. C. McIntosh, and D. A. Caldwell (2004), $^{40}Ar/^{39}Ar$ dating of the eruptive history of Mount Erebus, Antarctica: Summit flows, tephra, and caldera collapse, *Bull. Volcanol.*, *66*, 687–702, doi:10.1007/s00445-004-0349-7.

Hemming, S. R. (2004), Heinrich events: Massive late Pleistocene detritus layers of the North Atlantic and their global climate imprint, *Rev. Geophys.*, *42*, RG1005, doi:10.1029/2003RG000128.

Hemming, S. R., W. S. Broecker, W. D. Sharp, G. C. Bond, and J. F. Gwiazda (1998), Provenance of the Heinrich layers in core V28–82, northeastern Atlantic: $^{40}Ar$-$^{39}Ar$ ages of ice-rafted hornblende, Pb isotopes in feldspar grains, and Nd–Sr–Pb isotopes in the fine sediment fraction, *Earth Planet. Sci. Lett.*, *164*, 317–333, doi:10.1016/S0012-821X(98)00224-6.

Hemming, S. R., T. O. Vorren, and J. Kleman (2002), Provinciality of ice rafting in the North Atlantic: Application of $^{40}Ar/^{39}Ar$ dating of individual ice rafted hornblende grains, *Quaternary Int.*, *95–96*, 75–85, doi:10.1016/S1040-6182(02)00029-0.

Henjes-Kunst, F., and U. Schüssler (2003), Metasedimentary units of the Cambro-Ordovician Ross orogen in northern Victoria Land and Oates Land: Implications for their provenance and geotectonic setting from geochemical and Nd-Sr isotope data, *Terra Antarct.*, *10*, 105–128.

Hill, D. J., A. M. Haywood, R. C. A. Hindmarsh, and P. J. Valdes (2007), Characterizing ice sheets during the Pliocene: Evidence from data and models, in *Deep-time Perspectives on Climate Change: Marrying the Signal From Computer Models and Biological Proxies*, edited by M. Williams et al., pp. 517–578, Geol. Soc., London.

Huybrechts, P. (1993), Glaciological modeling of the Late Cenozoic East Antarctic ice sheet: Stability or dynamism?, *Geogr. Ann., Ser. A*, *75*, 221–238, doi:10.2307/521202.

Jacobsen, S. B., and G. J. Wasserburg (1980), Sm-Nd isotopic evolution of chondrites, *Earth Planet. Sci. Lett.*, *50*, 139–155, doi:10.1016/0012-821X(80)90125-9.

Jordan, T. A., F. Ferraccioli, H. Corr, A. Graham, E. Armadillo, and E. Bozzo (2010), Hypothesis for mega-outburst flooding from a palaeo-subglacial lake beneath the East Antarctic Ice Sheet, *Terra Nova*, *22*, 283–289.

Kennett, J. P. (1977), Cenozoic evolution of Antarctic glaciation, the circum-Antarctic Ocean, and their impact on global paleoceanography, *J. Geophys. Res.*, *82*, 3843–3860, doi:10.1029/JC082i027p03843.

Kennett, J. P., and N. J. Shackleton (1976), Oxygen isotopic evidence for the development of the psychrosphere 38 Myr ago, *Nature*, *260*, 513–515, doi:10.1038/260513a0.

Lear, C. H., H. Elderfield, and P. A. Wilson (2000), Cenozoic deep-sea temperatures and global ice volumes from Mg/Ca in benthic foraminiferal calcite, *Science*, *287*, 269–272, doi:10.1126/science.287.5451.269.

LeMasurier, W. E., and J. W. Thomson (1990), *Volcanoes of the Antarctic Plate and Southern Oceans*, *Antarct. Res. Ser.*, 487 pp., AGU, Washington, D. C.

Leventer, A., E. Domack, R. Dunbar, J. Pike, C. Stickely, E. Maddison, S. Brachfeld, P. Manley, and C. McClennan (2006), Marine sediment record from the East Antarctic margin reveals dynamic of ice sheet recession, *GSA Today*, *16*(12), 7, doi:10.1130/GSAT01612A.1.

Lewis, A. R., D. R. Marchant, D. E. Kowalewski, S. L. Baldwin, and L. E. Webb (2006), The age and origin of the Labyrinth, western Dry Valleys, Antarctica: Evidence for extensive middle Miocene subglacial floods and freshwater discharge to the Southern Ocean, *Geology*, *34*(7), 513–516, doi:10.1130/G22145.1.

Lewis, A. R., D. R. Marchant, A. C. Ashworth, S. R. Hemming, and M. L. Machlus (2007), Major middle Miocene global climate change: Evidence from East Antarctica and the Transantarctic Mountains, *GSA Bulletin*, *119*(11–12), 1449–1461.

Liu, X., B. Jahn, Y. Zhao, M. Li, H. Li, and X. Liu (2006), Late Pan-African granitoids from the Grove Mountains, East Antarctica: Age, origin and tectonic implications,*Precambrian Res.*, *145*, 131–154, doi:10.1016/j.precamres.2005.11.017.

Liu, X., Y. Zhao, G. Zhao, P. Jian, and G. Xu (2007), Petrology and geochronology of granulites from the McKaskle Hills, Eastern Amery Ice Shelf, Antarctica, and implications for the evolution of the Prydz Belt, *J. Petrol.*, *48*(8), 1443–1470, doi:10.1093/petrology/egm024.

Ludwig, K. R. (2003), *User's Manual for Isoplot/Ex Version 3.00: A Geochronological Toolkit for Microsoft Excel*, *Spec. Publ. 4*, p. 72, Berkeley Geochronology Cent., Berkeley, Calif.

Lythe, M. B., D. G. Vaughan, and the BEDMAP Consortium (2001), BEDMAP: A new ice thickness and subglacial topographic model of Antarctica, *J. Geophys. Res.*, *106*, 11,335–11,351, doi:10.1029/2000JB900449.

Marchant, D. R., G. H. Denton, D. E. Sugden, and C. C. Swisher III (1993), Miocene glacial stratigrapy and landscape evolution of the western Asgard range, Antarctica, *Geogr. Ann., Ser. A*, *75*, 303–330, doi:10.2307/521205.

Meert, J. G. (2003), A synopsis of events related to the assembly of eastern Gondwana, *Tectonophysics*, *362*, 1–40, doi:10.1016/S0040-1951(02)00629-7.

Ménot, R. P., G. Duclaux, J. J. Peucat, Y. Rolland, S. Guillot, M. Fanning, J. Bascou, D. Gapais, and A. Pêcher (2007), Geology of the Terre Adélie Craton (135–146°E), in *Antarctica: A Keystone in a Changing World: Proceedings of the 10th International Symposium on Antarctic Earth Sciences, Santa Barbara, California, August 26 to September 1, 2007*, edited by A. K. Cooper et al., p. 3, Natl. Acad., Washington, D. C.

Mercer, J. H. (1978), West Antarctic ice sheet and $CO_2$ greenhouse effect: A threat of disaster, *Nature*, *271*, 321–325, doi:10.1038/271321a0.

Miller, K. G., J. D. Wright, and J. V. Browning (2005), Visions of ice sheets in a greenhouse world, *Mar. Geol.*, *217*, 215–231, doi:10.1016/j.margeo.2005.02.007.

Möller, A., N. J. Post, and B. J. Hensen (2002), Crustal residence history and garnet Sm–Nd ages of high-grade metamorphic rocks from the Windmill Islands area, East Antarctica, *Int. J. Earth Sci.*, *91*, 993–1004, doi:10.1007/s00531-002-0291-x.

Palmeri, R., B. Ghiribelli, F. Talarico, and C. A. Ricci (2003), Ultra-high-pressure metamorphism in felsic rocks: The garnet-phengite gneisses and quarzites from the Lanterman Range, Antarctica, *Eur. J. Mineral.*, *15*, 513–525, doi:10.1127/0935-1221/2003/0015-0513.

Paulsen, T. S., and T. J. Wilson (2007), Elongate summit calderas as possible Neogene paleostress indicators in Antarctica, in *Antarctica: A Keystone in a Changing World: Proceedings of the 10th International Symposium on Antarctic Earth Sciences, Santa Barbara, California, August 26 to September 1, 2007*, edited by A. K. Cooper et al., p. 6, Natl. Acad., Washington, D. C.

Pekar, S. F., and R. M. DeConto (2006), High-resolution ice-volume estimates for the Early Miocene: Evidence for a dynamic ice sheet in Antarctica, *Palaeogeogr. Palaeoclimatol. Palaeoecol.*, *231*, 101–109, doi:10.1016/j.palaeo.2005.07.027.

Peucat, J. J., R. P. Ménot, O. Monnier, and C. M. Fanning (1999), The Terre Adélie basement in the East-Antarctica Shield: Geological and isotopic evidence for a major 1.7 Ga thermal event; comparison with the Gawler Craton in south Australia, *Precambrian Res.*, *94*, 205–224, doi:10.1016/S0301-9268(98)00119-3.

Phillips, G., C. J. L. Wilson, D. Phillips, and S. K. Szczepanski (2007), Thermochronological ($^{40}Ar/^{39}Ar$) evidence of Early Paleozoic basin inversion within the southern Prince Charles Mountains, East Antarctica: Implications for east Gondwana, *J. Geol. Soc.*, *164*, 771–784, doi:10.1144/0016-76492006-073.

Pollard, D., and R. M. DeConto (2009), Modelling West Antarctic ice sheet growth and collapse through the past five million years, *Nature*, *458*, 329–332, doi:10.1038/nature07809.

Post, N. J. (2000), *Unravelling Gondwana Fragments: An Integrated Structural, Isotopic and Petrographic Investigation of the Windmill Islands, Antarctica*, Univ. of N. S. W., Kensington.

Post, N. J., B. J. Hensen, and P. D. Kinny (1996), Two metamorphic episodes during a 1340–1180 Ma convergent tectonic event in the Windmill Islands, East Antarctica, in *The Antarctic Region: Geological Evolution and Processes: Proceedings of the 7th International Symposium on Antarctic Earth Sciences*, edited by C. A. Ricci, pp. 157–161, Terra Sci., Siena, Italy.

Reiners, P. W., T. A. Ehlers, and P. K. Zeitler (2005), Past, present, and future of thermochronology, *Rev. Mineral. Geochem.*, *58*, 1–18, doi:10.2138/rmg.2005.58.1.

Rocchi, S., S. Tonarini, P. Armienti, F. Innocenti, and P. Manetti (1998), Geochemical and isotopic structure of the early Palaeozoic active margin of Gondwana in northern Victoria Land, Antarctica, *Tectonophysics*, *284*, 261–281, doi:10.1016/S0040-1951(97)00178-9.

Roy, M., T. van de Flierdt, S. R. Hemming, and S. L. Goldstein (2007), $^{40}$Ar/$^{39}$Ar ages of hornblende grains and bulk Sm/Nd isotopes of circum-Antarctic glacio-marine sediments: Implications for sediment provenance in the Southern Ocean, *Chem. Geol.*, *244*, 507–519, doi:10.1016/j.chemgeo.2007.07.017.

Ruddiman, W. F. (1977), Late Quaternary deposition of ice-rafted sand in the subpolar North Atlantic (lat 40° to 65°N), *Geol. Soc. Am. Bull.*, *88*, 1813–1827, doi:10.1130/0016-7606(1977)88<1813:LQDOIS>2.0.CO;2.

Rudnick, R. L., and S. Gao (2003), Composition of the continental crust, in *Treatise on Geochemistry*, edited by H. D. Heinrich and K. K. Turekian, pp. 1–64, Elsevier, Amsterdam, doi:10.1016/B0-08-043751-6/03016-4.

Samson, S. D., and E. C. Alexander (1987), Calibration of the interlaboratory $^{40}$Ar/$^{39}$Ar dating standard, MMhb-1, *Chem. Geol.*, *66*, 27–34.

Schoof, C. (2007), Ice sheet grounding line dynamics: Steady states, stability, and hysteresis, *J. Geophys. Res.*, *112*, F03S28, doi:10.1029/2006JF000664.

Schüssler, U., M. Brocker, F. Henjes-Kunst, and H. T. Will (1999), P-T-t evolution of the Wilson Terrane metamorphic basement at Oates Coast, Antarctica, *Precambrian Res.*, *93*, 235–258.

Shackleton, N. J., and J. P. Kennett (1975), Late Cenozoic oxygen and carbon isotope changes at DSDP site 284: Implications for glacial history of the Northern Hemisphere and Antarctica, *Initial Rep. Deep Sea Drill. Proj.*, *29*, 801–807.

Sheraton, J. W., L. P. Black, M. T. McCulloch, and R. L. Oliver (1990), Age and origin of a compositionally varied mafic dyke swarm in the Bunger Hills, East Antarctica, *Chem. Geol.*, *85*, 215–246, doi:10.1016/0009-2541(90)90002-O.

Sheraton, J. W., L. P. Black, and A. G. Tindle (1992), Petrogenesis of plutonic rocks in a Proterozoic granulite-facies terrane–The Bunger Hills, East Antarctica: Chemical Geology, *Chem. Geol.*, *97*, 163–198, doi:10.1016/0009-2541(92)90075-G.

Shevenell, A. E., J. P. Kennett, and D. W. Lea (2004), Middle Miocene Southern Ocean cooling and Antarctic cryosphere expansion, *Science*, *305*, 1766–1770, doi:10.1126/science.1100061.

Siegert, M. J., S. Carter, I. Tabacco, S. Popov, and D. D. Blankenship (2005a), A revised inventory of Antarctic subglacial lakes, *Antarct. Sci.*, *17*(3), 453–480, doi:10.1017/S0954102005002889.

Siegert, M. J., J. Taylor, and A. J. Payne (2005b), Spectral roughness of subglacial topography and implications for former ice-sheet dynamics in East Antarctica, *Global Planet. Change*, *45*, 249–263, doi:10.1016/j.gloplacha.2004.09.008.

Stüwe, K., and R. Oliver (1989), Geological history of Adé1ie Land and King George V Land, Antarctica: Evidence for a polycyclic metamorphic evolution, *Precambrian Res.*, *43*, 317–334, doi:10.1016/0301-9268(89)90063-6.

Tanaka, T., et al. (2000), JNdi-1: A neodymium isotopic reference in consistency with LaJolla neodymium, *Chem. Geol.*, *168*, 279–281, doi:10.1016/S0009-2541(00)00198-4.

Taylor, S. R., and S. M. McLennan (1995), The geochemical evolution of the continental crust, *Rev. Geophys.*, *33*(2), 241–265, doi:10.1029/95RG00262.

Tong, L., X. Liu, L. Zhang, and H. Chen (1998), The $^{40}$Ar-$^{39}$Ar ages of hornblendes in Grt-Pl-bearing amphibolite from the Larsemann Hills, East Antarctica and their geological implications, *Chin. J. Polar Sci.*, *9*(2), 79–91.

Tong, L., C. J. L. Wilson, and X. Liu (2002), A high-grade event of ~1100 Ma preserved within the ~500 Ma mobile belt of the Larsemann Hills, East Antarctica: Further evidence from $^{40}$Ar-$^{39}$Ar dating, *Terra Antarct.*, *9*, 73–86.

van de Flierdt, T., S. R. Hemming, S. L. Goldstein, G. E. Gehrels, and S. E. Cox (2008), Evidence against a young volcanic origin of the Gamburtsev Subglacial Mountains, Antarctica, *Geophys. Res. Lett.*, *35*, L21303, doi:10.1029/2008GL035564.

Vaughan, D., J. Bamber, M. Giovinetto, J. Russel, and A. Cooper (1999), Reassessment of net surface mass balance in Antarctica, *J. Clim.*, *12*, 933–946, doi:10.1175/1520-0442(1999)012<0933:RONSMB>2.0.CO;2.

Veevers, J. J. (2003), Pan-African is Pan-Gondwanaland: Oblique convergence drives rotation during 650–500 Ma assembly, *Geology*, *31*(6), 501–504, doi:10.1130/0091-7613(2003)031<0501:PIPOCD>2.0.CO;2.

Veevers, J. J. (2004), Gondwanaland from 650–500 Ma assembly through 320 Ma merger in Pangea to 185–100 Ma breakup: Supercontinental tectonics via stratigraphy and radiometric dating, *Earth Sci. Rev.*, *68*, 1–132, doi:10.1016/j.earscirev.2004.05.002.

Williams, T., T. van de Flierdt, E. Chung, M. Roy, S. R. Hemming, and S. L. Goldstein (2010), Major Miocene changes in East Antarctica ice sheet dynamics revealed by iceberg provenance, *Earth Planet. Sci. Lett.*, *290*, 351–361, doi:10.1016/j.epsl.2009.12.031.

Wilson, C. L. J., C. Quinn, L. Tong, and D. Phillips (2007), Early Paleozoic intracratonic shears and post-tectonic cooling in the Rauer Group, Prydz Bay, East Antarctica constrained by $^{40}$Ar/$^{39}$Ar thermochronology, *Antarct. Sci.*, *19*(03), 339–353, doi:10.1017/S0954102007000478.

Wingham, D. J., M. J. Siegert, A. Shepherd, and A. S. Muir (2006), Rapid discharge connects Antarctic subglacial lakes, *Nature*, *440*, 1033–1036, doi:10.1038/nature04660.

Zachos, J. C., J. R. Breza, and S. W. Wise (1992), Early Oligocene ice-sheet expansion on Antarctica; stable isotope and sedimentological evidence from Kerguelen Plateau, southern Indian Ocean, *Geology*, *20*, 569–573, doi:10.1130/0091-7613(1992)020 < 0569:EOISEO > 2.3.CO;2.

Zachos, J. C., K. C. Lohmann, J. C. G. Walker, and S. W. Wise (1993), Abrupt climate change and transient climates during the Paleogene: A marine perspective, *J. Geol.*, *101*, 191–213, doi:10.1086/648216.

Zachos, J. C., M. Pagani, L. Sloan, E. Thomas, and K. Billups (2001), Trends, rhythms and aberrations in global climate 65 Ma to present, *Science*, *292*, 686–693, doi:10.1126/science.1059412.

Zhao, Y., X. H. Liu, S. C. Wang, and B. Song (1997), Syn- and post-tectonic cooling and exhumation in the Larsemann Hills, East Antarctica, *Episodes*, *20*(2), 122–127.

Zhao, Y., X. H. Liu, X. C. Liu, and B. Song (2003), Pan-African events in Prydz Bay, East Antarctica, and their implications for East Gondwana tectonics, *Geol. Soc. Spec. Publ.*, *206*, 231–245.

S. A. Brachfeld, Department of Earth and Environmental Studies, Montclair State University, Montclair, NJ 07043, USA.

S. L. Goldstein, S. R. Hemming, and T. Williams, Lamont-Doherty Earth Observatory, 61 Rt. 9W, Palisades, NY 10964, USA.

E. L. Pierce, Department of Earth and Environmental Sciences, Columbia University, 2960 Broadway, New York, NY 10025, USA. (epierce@ldeo.columbia.edu)

T. van de Flierdt, Department of Earth Science and Engineering, Imperial College London, London SW7 2AZ, UK.